On the Electromagnetic Fields from a Hybrid Type of EMP Simulator

RONALD F. BLACKBURN, MEMBER, IEEE, AND CLAYBORNE D. TAYLOR, MEMBER, IEEE

Abstract—A typical hybrid type of EMP simulator that is used in the simulation of the nuclear electromagnetic pulse is analyzed. Because of the width of the pulse frequency spectrum, the behavior of the antenna is determined separately for three specific frequency regimes. Also, the pulse-power source interaction with the antenna is considered. After the frequency response of the antenna is determined, Laplace transform theory is utilized to obtain the pulse response.

Experimental data are compared with theoretical predictions.

Key Words: EMP simulator, hybrid, EM fields, theory, experiment.

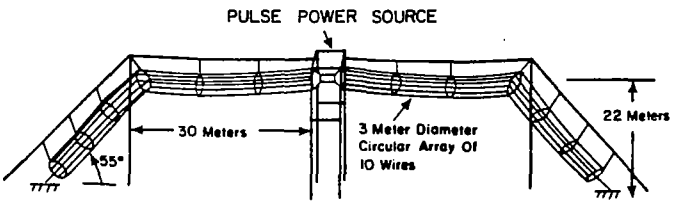

Fig. 1. Illustration of the ACHILLES II EMP simulator facility, Kirtland AFB, New Mexico.

INTRODUCTION

THE SIMULATION of the nuclear electromagnetic pulse (EMP) requires the radiation of energy over an extremely broad frequency band. Presently, EMP simulators may be separated into three classes: the bounded-wave simulator or transmission line, the open radiator, and the hybrid simulator [1]. The bounded-wave simulator possesses many desirable characteristics, including spatial uniformity of the simulator fields, faithful simulation of the EMP pulse shape, and high field strengths [2]-[6]. Undesirable characteristics of these simulators include having a limited test volume, exhibiting significant simulator/test-object interaction, and being nonportable. Desirable characteristics of the open radiator include portability and virtually unlimited test volume. But the many undesirable characteristics include insufficient field strengths and insufficient low-frequency content of the simulated EMP. The hybrid-type simulator is designed to overcome the aforementioned deficiencies of the open radiator, yet maintaining many of its advantages. While the hybrid simulator generally behaves at low frequency as a transmission line, at high frequency it behaves like an open radiator.

Several hybrid-type simulators have been constructed and are presently in use. Two such facilities, referred to as the ACHILLES II and the ATHAMAS simulators,[1] are being used for testing aircraft and missiles at Kirtland AFB, New Mexico. See Fig. 1 for an illustration of the ACHILLES II simulator. Other hybrid-type simulators that are in use include the EMPRESS and NAVES I, operated by the Navy Surface Weapons Center, and the TEMPS, operated by the Harry Diamond Laboratory.

Manuscript received November 12, 1975; revised September 26, 1977.

R. F. Blackburn is with the Air Force Weapons Laboratory, Kirtland AFB, NM 87115.

C. D. Taylor is with the Departments of Electrical Engineering and Physics, Mississippi State University, Starkville, MS 39762. (601) 325-6064.

[1] These simulators are also referred to as the SRF and HPD, respectively.

The bounded-wave simulator has received a great deal of attention; however, the open-radiator and hybrid simulators have not been studied so extensively [7]-[10]. In particular, the electromagnetic field from the hybrid simulator has not been determined theoretically for the complete frequency band necessary for EMP simulation. This paper, however, does present such an analysis that uses three different formulations for three portions of the EMP frequency spectrum.

A theoretical formulation is required for understanding, as well as predicting, the electromagnetic field produced by the simulator. And, due to the point-to-point variation in the field components, a theoretical formulation is needed to supplement the field measurements. Moreover, the electrical response of a test object in the facility is more easily obtained if the simulator fields can be calculated directly.

Some experimental data taken at the ACHILLES II simulator facility are presented. Corresponding theoretical data are also presented for comparison. In general, the agreement verifies the analysis.

ANALYSIS

The purpose of this paper is to present techniques for analyzing the hybrid type of EMP simulator and to analyze the performance of the ACHILLES II simulator located at Kirtland AFB, New Mexico. In order to develop the theoretical analysis, the frequency spectrum of the EMP is divided into three portions, hereafter referred to as the low-frequency regime, the mid-frequency regime, and the high-frequency regime. Rather than presenting the formulation of hybrid-type simulators in a most general form, the specific analysis of the ACHILLES II simulator will be presented.

In Fig. 1, the geometrical configuration of the typical hybrid simulator is illustrated. An appropriate pulse-power source for the simulator is a Marx generator, a capacitive-discharge surge generator. For a biconical section in the vicinity of the pulser, the antenna impedance seen by the pulser is simply the charac-

0018-9375/78/0200-0240$00.75

SENSOR AND SIMULATION NOTES

Note 211

November 1975

ON THE ELECTROMAGNETIC FIELDS FROM A HYBRID TYPE OF EMP SIMULATOR

by

Ronald F. Blackburn

Air Force Weapons Laboratory
Kirtland AFB, New Mexico 87115

Clayborne D. Taylor
Mississippi State University
Mississippi State, Mississippi 39762

ABSTRACT

A resistively loaded loop antenna used in the simulation of the nuclear electromagnetic pulse is analyzed. Because of the width of the pulse frequency spectrum the behavior of the antenna is determined separately for three specific frequency regimes. Also the pulse-power source interaction with the antenna is considered. After the frequency response of the antenna is determined Laplace transform theory is utilized to obtain the pulse response.

Experimental data are compared with theoretical predictions.

INTRODUCTION

The simulation of the nuclear EMP (electromagnetic pulse) requires the radiation of energy over an extremely broad frequency band. At present there are basically three classes of EMP simulators: the bounded wave simulator or transmission line, the open radiator and the hybrid simulator [1]. The hybrid simulator generally behaves at low frequency as a transmission line and at high frequency as an open radiator. The bounded wave simulator, e.g., the parallel plate transmission line, has received a great deal of attention [2, 3, 4 and 5]. However the open radiator and hybrid simulator have not been studied as extensively [6, 7, 8, 9]. In particular the electromagnetic field from the hybrid radiator has not been determined theoretically for the complete frequency band necessary for EMP simulation. This report, however, does present such a theoretical study requiring three different formulations for the three portions of the EMP frequency spectrum.

Some experimental data taken at the ACHILLES II simulator facility of Kirtland AFB, New Mexico is presented.* Corresponding theoretical data are also presented for comparison. In general the agreement verifies the analysis.

---

*This simulator facility is also referred to as the SRF facility.

ANALYSIS

The purpose of this report is to present techniques for analyzing the hybrid type of EMP simulator and to analyze the performance of the ACHILLES II simulator located at Kirtland AFB, New Mexico [10]. In order to develop the analysis the frequency spectrum of the EMP is divided into three portions, hereafter referred to as the low frequency regime, mid-frequency regime and the high frequency regime. Rather than presenting the formulation in a most general form it will be directed toward the specific analysis of the aforementioned simulator.

In figure 1 the geometrical configuration of the SRF simulator is shown. An appropriate pulse-power source for the simulator is a Marx generator, a capacitive discharge pulser. By using a biconical section in the vicinity of the pulser the antenna impedance seen by the pulser is simply the characteristic impedance of the biconical transmission line for the initial time interval occurring until the first reflection of the launched current pulse is observed. If a smooth transition is made between the biconical input section and the remaining cylindrical section then the reflection from this transition region will be essentially negligible. Unfortunately this may not have been realized in the construction of the ACHILLES facility. See figure 2 for the dimensions of the biconical input section for the ACHILLES antenna.

Inserting series resistors along the length of the antenna increases its bandwidth. The resistors tend to eliminate the production of a standing wave pattern on the antenna. Associated with standing waves are resonances and antiresonances in a manner completely analogous to open-ended or shorted

transmission lines. To be most effective the values of the resistors should increase with distance from the input section and the first resistor should have a resistance appreciably less than the characteristic impedance of the biconical input section. For a more complete discussion of the resistive loading the authors defer to ref. 6 and 9.

In order to determine the electromagnetic pulse produced by the hybrid type of EMP simulator, the behavior of the antenna is determined in the frequency domain and the Laplace transform theory is used to time domain behavior. This technique requires that the Laplace transform of the input voltage pulse be known. Hence an analysis of the pulse-power source is required.

1. PULSE-POWER SOURCE

The equivalent circuit of the pulse-power source for the ACHILLES II is [10]

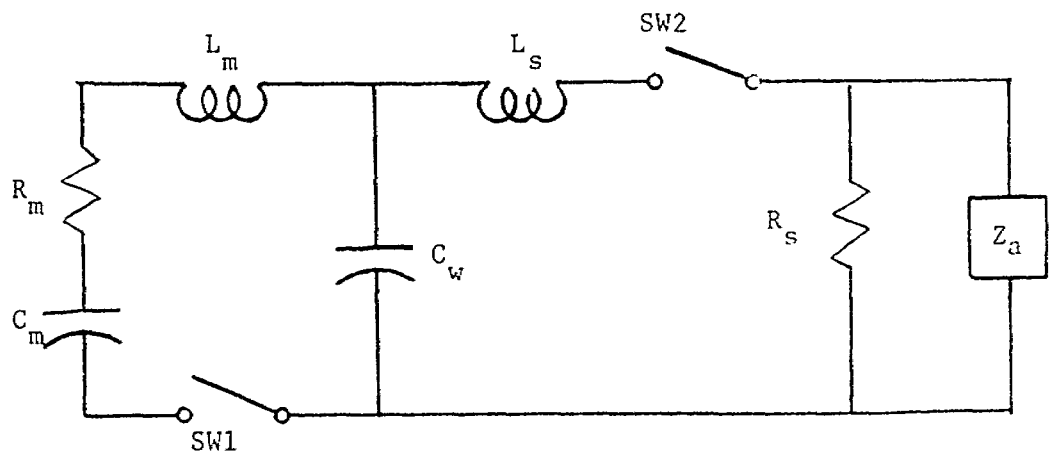

where $L_m \simeq 175\ \mu H$, $L_s \simeq 0.35\ \mu H$, $R_m \simeq 100\ \Omega$, $C_w \simeq 750$ pF, $C_m = 3125$ pF, and $R_s \simeq 5$ K . Here Z_a, the antenna impedance, is the load impedance as seen by the source. The procedure for firing the pulser involves first the closing of SW1 at $t = 0$ while SW2 is closed at a later time $t = t_1$,

the time the voltage across capacitor C_W reaches its maximum value. For the foregoing circuit it is readily shown that the Thevenin equivalent voltage and impedance of the pulse-power source are

$$V_{TH} = \frac{[v_c(0) + C_W v_{cW}(R_m s + L_m s^2)]R_s}{L_s L_m C_W s^4 + (R_s L_m + R_m L_s)C_W s^3 + (L_m + \frac{L_s C_W}{C_T} + R_m R_s C_W)s^2 + (R_m + \frac{R_s C_W}{C_T})s + \frac{1}{C_m}}$$

$$Z_{TH} = \frac{R_s(Z_1 + sL_s)}{Z_1 + R_s + sL_s}$$

where

$$Z_1 = \frac{R_m + sL_m + \frac{1}{sC_m}}{L_m C_W s^2 + R_m C_W s + \frac{C_W}{C_T}]}$$

$$C_T = \frac{C_m C_W}{C_m + C_W}$$

$$v_{cW} = \frac{C_T}{C_W} v_c(0)(1 - e^{-at_1})$$

$$v_{cm} = v_c(0)[1 - \frac{C_T}{C_m}(1 - e^{-at_1})]$$

$$a = \frac{R_m}{2L_m}$$

$$t_1 = \pi / \sqrt{\frac{1}{L_m C_T} - a^2}$$

Here $v_c(0)$ is the initial voltage across the C_m capacitor. Initially the C_W capacitor is uncharged

If the antenna impedance is known then the antenna voltage may be obtained from

$$V_a = \frac{V_{TH} Z_a}{Z_{TH} + Z_a}$$

At low frequencies, $|s|^4 << (L_s L_m C_W C_m)^{-1}$,

$$Z_a \simeq 2R_L \text{(total load resistance in loop)}$$

$$\simeq 1.12\ K\Omega$$

and the antenna voltage is approximately

$$V_a \simeq v_c(0) \frac{(1 - e^{-at_1})^{-1}}{s + \frac{1}{R_m C_m + Z_s(C_m + C_W)}}$$

where

$$Z_s = \frac{R_s Z_a}{R_s + Z_a} \simeq 914\ \Omega$$

At high frequencies, $|s|^4 >> (L_s L_m C_W C_m)^{-1}$,

$$Z_a \simeq C_c \text{ (characteristic impedance of the bicone feed section)}$$

$$\simeq 158\ \Omega$$

and the corresponding antenna voltage is

$$V_a \simeq v_{C_W} \frac{\frac{Z_s}{L_s}}{s(s + \frac{Z_s}{L_s})}$$

where

$$Z_s = \frac{R_s Z_a}{R_s + Z_a} \simeq 153\ \Omega$$

Both the high frequency and low frequency approximations for the applied antenna voltage may be combined as

$$V_a \simeq \frac{\alpha V_o}{(s + \alpha)(s + \beta)} \tag{1}$$

where

$$V_o \simeq v_{cW} = 1.75 \times 10^6\ V$$

$$\alpha \simeq \left.\frac{Z_s}{L_s}\right|_{Z_s = 153\ \Omega} = 4.4 \times 10^8$$

$$\beta \simeq \left.\frac{1}{R_m C_m + Z_s(C_W + C_m)}\right|_{Z_s = 914\ \Omega} = 2.6 \times 10^5$$

The foregoing provides a rough approximation to the antenna voltage appropriate for the ACHILLES II facility. A more accurate result would require a knowledge of the antenna impedance over the EMP frequency spectrum. The time history of the antenna voltage as obtained using (1) is

$$v_a(t) \simeq \frac{\alpha V_o}{\alpha - \beta}\left[e^{-\beta t} - e^{-\alpha t}\right] \tag{2}$$

In analyzing the behavior of the ACHILLES II three frequency regimes are identified and the behavior of the antenna determined for each regime using the applied voltage as shown in (1) and (2).

2. HIGH FREQUENCY REGIME ANALYSIS

In the time interval before the pulse eminating from the source reaches the edge of the conical input section the radiation is exactly that which would occur if the radiator were a biconical antenna. The electric field has only a theta component and the magnetic field has only a phi component as illustrated in figure 3. It is [11]

$$E_\theta(r,\theta,s) = \frac{\eta\, V_a(s)}{2\pi r\, Z_c \sin\theta}\, e^{-sr/c} \qquad (3)$$

$$H_\phi(r,\theta,s) = \frac{1}{\eta}\, E_\theta(r,\theta,s)$$

where

$$\eta = \sqrt{\mu/\epsilon} \simeq 120\,\pi\ \Omega \text{ for free space}$$

$$c = 1/\sqrt{\mu\epsilon}$$

$$Z_c = \frac{\eta}{\pi} \ln \cot \frac{\theta_o}{2} \,]$$

Moreover the foregoing is approximately valid for the time interval required for the pulse emerging from the biconical input section to reach the first resistor, 12 m from the apex of the bicone. Hence the field expressions are adequate for the time interval

$$0 \leq t \leq \frac{12\ \text{m}}{c}$$

or for frequencies satisfying

$$f \gtrsim \frac{4}{\frac{12\ \text{m}}{c}} = 100\ \text{mHz}$$

or

$$|s| \geq 6 \times 10^8 \text{ sec}^{-1}$$

However the foregoing is not complete. In addition to the direct field from the pulser there is also a field contribution from the image of the pulser with the polarity of the image pulser reversed.

3. MIDFREQUENCY REGIME ANALYSIS

As the pulse eminating from the generator propagates along the antenna structure it is attenuated by radiation power loss and ohmic power loss in the load resistors. In the midfrequency regime this power loss is to such an extent that the current on the vertical legs is considerably less than that occurring near the pulser. Because of this effect it is possible to consider again an antenna structure somewhat modified to facilitate analysis. In particular, the vertical sections are considered colinear with the horizontal section so that the antenna structure becomes a resistively loaded dipole oriented parallel to the ground plane.

By using Schelkunoff's transmission line model for a linear antenna Baum [7] has obtained the electric field radiated from a restively loaded dipole as

$$E_\theta(r,\theta,s) = \frac{\eta\, s_h\, V_a(s)}{2\pi\, Z_\infty r \sin\theta} \frac{f(\theta,h,s)}{s_h + B/\sin^2\theta} e^{-sr/c} \qquad (5)$$

where

$$f(\theta,h,s) = 1 - \frac{e^{s_h\cos\theta} + e^{-s_h\cos\theta}}{e^{\gamma_h} + e^{-\gamma_h}}$$

$$s_h = s\,h/c$$

$$\gamma_h = s_h + B/2$$

$$B = R_L/Z_\infty$$

and Z_∞ is the characteristic impedance appropriate for the transmission line model. Actually the foregoing expression, equation (5), is obtained from Baum's result by considering f > 17 mHz or $|s| > 10^8$ sec^{-1}. For the ACHILLES II antenna model h = 56.4 m and R_L = 559.2 Ω. The theta component of the electric field is exhibited in fig. 3.

In deriving the expression for the electric field Baum [7] considered the resistive loading to be uniform rather than lumped as shown in figure 4. Thus the analysis is valid only for frequencies with wavelengths appreciably greater than the separation of the resistive loads. Hence the results are valid for frequencies approaching the lower limit of the high frequency analysis in the foregoing section. If characteristic impedance, Z_c, in the mid-frequency expression for the electric field is set equal Z_c of the corresponding high frequency formula, then the mid-frequency formula, equation (5), is essentially equivalent to the corresponding high frequency formula, equation (3), provided f ≥ 100 mHz.

However the mid-frequency analysis is valid only if the current is considerably attenuated away from the pulse-power source. Ascertaining the attenuation requires the solution be obtained for the current distribution. This was done as part of the low frequency solution to be presented subsequently. From the low frequency solution for the ACHILLES II antenna it is determined that the antenna current is considerably attenuated

for frequencies of the order of and greater than 17 mHz, thus determining a suitable low frequency limit of the mid-frequency analysis.

Again the proximity to the ground plane must be considered. It is convenient to use image theory noting that the voltage source for the image is reversed.

4. LOW FREQUENCY REGIME ANALYSIS

This frequency regime is perhaps the most difficult to analyze. First it requires the solution of an integral equation for the antenna current distribution. The Hallén-type integral equation for the antenna current on thin wire structures is [12]

$$\int_L d\ell' I(\ell') \Pi(\ell,\ell') = C_1 \cos k\ell + C_2 \sin k\ell - j\frac{4\pi}{\eta}\int_0^{\ell} d\xi\, E_\ell^{inc}(\xi) \sin k(\ell - \xi) \qquad (6)$$

where

$$\Pi(\ell,\ell') = K(\ell,\ell')\,\hat{\ell}\cdot\hat{\ell} - \int_0^{\ell} d\xi \{ \frac{\partial}{\partial \xi} [\hat{\xi}\cdot\hat{\ell}'\, K(\xi,\ell')] + \frac{\partial}{\partial \ell'} K(\xi,\ell') \} \cos k(\ell - \xi)$$

$$K(\ell,\ell') = \exp[-jk\sqrt{R^2(\ell,\ell') + a^2}]/\sqrt{R^2(\ell,\ell') + a^2}$$

$$k = -js/c$$

Here $I(\ell')$ is the antenna current at point ℓ' along the antenna, $R(\ell,\ell')$ is the linear distance between points ℓ and ℓ' along the antenna structure,

$\hat{\ell}$ is the unit vector tangent to the antenna axis at point ℓ and is directed toward increasing ℓ, and $E_{\ell}^{inc}(\xi)$ is the component of the incident or impressed electric field tangent to the antenna axis at point ξ along the antenna (see figure 5). For a source generator located at $\ell = \ell_o$ the impressed field is

$$E_{\ell}^{inc}(\xi) = -V_o \, \delta(\xi - \ell_o)$$

and for a load impedance Z_o located at $\ell = \ell_o$, the compensation theorem may be used, i.e. the impressed field becomes

$$E_{\ell}^{inc}(\xi) = +I(\ell_o)Z_o \, \delta(\xi - \ell_o)$$

Hence by using superposition and the compensation theorem any number of generators and loads can be analyzed.

If the antenna is composed of straight wire segments that are either perpendicular or parallel, then equation (6) is greatly simplified. As seen from figure 1 the ACHILLES II antenna with its image is not composed of parallel and perpendicular segments. However, to facilitate the analysis and equivalent rectangular loop is considered. It is equivalent in that the input generator sections are the same heights above the ground and that the total wire lengths or antenna lengths are the same (see figure 5). Of course the rectangular loop has a smaller area than the actual ACHILLES II antenna but this difference is less than 10 percent. Hence the rectangular loop model should yield acceptable results

The antenna current distribution may be obtained numerically by using the method of moments. Considering the rectangular loop antenna with multiple sources and load impedances, Fyke and Butler [13] have solved for

the current using the aforementioned technique. In their solution technique Fyke and Bulter represent the unknown current as a piecewise sinusoid. Because of the thin wire assumption the sinusoid zones had to have a length greater than or equal to 4a and in order to represent the current accurately at least 5 zones per wave length are needed. Thus the formulation has an upper limit in frequency for which it is valid. Accordingly it is

$$f \lesssim \frac{c}{20a}$$

or

$$f \lesssim 15 \text{ mHz}$$

but there is no low frequency limit. Hence the computer code developed by Fyke and Butler is modified appropriately to fit the rectangular loop model of the ACHILLES II antenna and thus complete the theoretical analysis.

The electromagnetic field about the loop antenna may be obtained directly from the antenna current distribution. To accomplish this the antenna is divided into short segments. It is well known that the dipole moment of a short current segment is

$$P = \frac{1}{s} I(\ell)\Delta\ell$$

where $\Delta\ell$ is the length of the current segment with current $I(\ell)$. The direction of the dipole moment is the direction of positive current on the segment. Using the dipole moment fields and vector addition it is straight forward to calculate all the field components about the antenna. Both the near field as well as the far field may be determined [14].

5. COMBINING THE APPROXIMATIONS FOR THE LAPLACE TRANSFORM

In dividing the frequency spectrum into 3 regions and obtaining the antenna field approximately for each regime the final result for the Laplace transform exhibits discontinuities in both amplitude and phase where the solutions join. These discontinuities affect the time domain results by superimposing a sinusoidal ripple on the time history and by violating casualty. Of course if exact solutions were obtained for each frequency regime there would be no such discontinuities. In an effort to eliminate this effect the midfrequency formula for the radiated electric field is required to match in amplitude and phase the high frequency approximation at the joining frequency. Since the midfrequency approximation is highly oscillatory the results obtained appeared to be a function of the frequency at which the approximations were joined. However it is found that by joining the formulas at a maximum point in the midfrequency approximation consistent results relatively insensitive to the joining frequency were obtained. The discontinuity between the low frequency and midfrequency formulas was not smoothed.

NUMERICAL RESULTS

As mentioned in the foregoing experimental data has been obtained for the electric and magnetic fields produced by the ACHILLES II facility. The data reported here have not been documented elsewhere. However, the accuracy of the data as well as measurement procedures are presented in ref. 15 along with some independently obtained data. These data are used to verify the theoretical formulation described in the preceding section. Points at which electric and magnetic field data were obtained are shown in figure 7. Positions 1 through 5 are at the same height above the ground, 2 meters. Position 6 is 12 meters above the ground. The electrical properties of the ground at the facility are not known precisely. Where the field measurements were taken the ground consisted of a concrete pad with steel rebar with a sparse wire mesh covering the pad (see ref. 16), while the theory considered a perfectly conducting ground. The related differences in the experimental and theoretical results will be pointed out.

In figure 8 the time histories are presented for the measured and calculated electric field components along the x-axis at position 1.* It is noted that the measured peak field differs from the calculated value less than 10% while the initial pulse shapes are essentially the same. Also readily observed in the calculated data is a second pulse occurring about 190 ns after the arrival of the first pulse. This second pulse arises from the inaccuracies of the midfrequency analysis. It physically represents the radiation occurring when the antenna current pulse is reflected from the open ends of the antenna structure. There are no open ends in the actual facility. Nevertheless the agreement between the calculated and measured time histories is quite satisfactory. This

agreement is perhaps more clearly exhibited in the resulting Fourier transforms of the aforementioned field components as seen in figure 9.

The experimental data reported here were obtained at slightly different positions than is indicated in the foregoing (a 10 to 20 percent variation is expected). However, the resulting differences in the data would make negligible changes in the figures that are presented. Also the Fourier transform of the experimental data is presented for frequencies beyond its theoretical limits of validity. Because of the finite time duration of the recorded data the Fourier transform yields data that are not valid below 4-11 mHz. Moreover the digitization of the time domain experimental data used to obtain the Fourier transform yields data that are not valid for frequencies above 100 mHz.

The time histories of the y components of the magnetic field at position 1 are shown in figure 10. The second peaks, more pronounced in the theoretical data, represents the pulse reflected from the ground. Because of the imperfect ground at the ACHILLES facility the measured data exhibits a second peak about 4/10 of the initial peak whereas the calculated second peak is about 9/10 of the initial peak. Otherwise time histories are quite similar. The agreement between the Fourier transforms of the y components of the magnetic fields is shown in figure 11.

In figure 12 the time histories of the z components of the magnetic field at position 1 are shown. The agreement between the initial pulses as calculated and measured is extremely good. Corresponding comparison of the Fourier transforms is exhibited in figure 13.

At position 1, as well as 4, 5 and 6, the y and z components of the electric field and the x component of the magnetic field are negligible

in comparison with the other field components. Because of the existing symmetry the y and z components of the fields observed at position 2 are exactly the same as observed at position 3. The corresponding x components are only reversed in direction. Also at positions 2 and 3 the time history of E_y is no longer negligible and is essentially the same as E_x but about 1/3 of the amplitude. The same observation is true as well for H_x and H_y. It also should be mentioned that the field amplitudes are greater for the positions nearer the pulse-power source. For example at position 4 the peak E_x value is 6.15 kV/m and at position 5 the peak E_x value is 1.35 kV/m.

In figure 14 the time histories of E_x are presented for positions 2 and 3. Because of experimental error different time histories were observed at the two points. These are shown to illustrate the expected accuracy of the measured data. Corresponding Fourier transforms are shown in figure 15. At positions 2 and 3 another field component becomes significant. It is the z component of the electric field. The measured and calculated time histories are shown in figure 16. There was essentially no difference in the measured data taken at the two positions. Note that although this waveform is also faithfully predicted by theory it is considerably different from the previously presented waveforms. This component of the electric field is significant for about 300 ns, in contrast with the electric field pulses that are significant for only a few nanoseconds. Corresponding Fourier transforms of the E_z pulses are shown in figure 17.

Calculated data are also presented for position 6, a height of 12 meters above the ground. At this height a significant broadening of the E_x pulse is observed in figure 18. The corresponding Fourier transform is exhibited in figure 19. In figure 20 the y component of the magnetic field exhibits

essentially the same time behavior as observed near the ground. The Fourier transform is presented in figure 21. But in figure 22 it is seen that the H_z pulse is considerably broadened as is observed for the E_x pulse. The corresponding Fourier transform is presented in figure 23.

CONCLUSION

A theoretical formulation is presented for understanding as well as predicting the electromagnetic field behavior in a hybrid EMP simulator facility. Because of the tremendous variation in the field components a theoretical formulation is also needed to supplement the field measurements. Moreover the electrical response of an object in the facility is more easily obtained if the simulator fields can be calculated directly. From the data obtained the response of an object may depend upon the orientation of the object as well as its location in the facility. This is a matter for future study.

The midfrequency analysis used in the theoretical study perhaps should be improved and this topic is reserved for future study.

ACKNOWLEDGEMENT

The authors wish to express appreciation to Dr. Carl Baum and Mr. Bill Kehrer of the Air Force Weapons Laboratory for their assistance in the preparation of this paper.

REFERENCES

1. Baum, C. E., "EMP Simulators for Various Types of Nuclear EMP Environments: An Interim Categorization," Sensor and Simulation Note 151, July 1972.

2. Carlisle, G. W., "Matching the Impedance of Multiple Transistions to a Parallel-Plate Transmission," Sensor and Simulation Note 54, Air Force Weapons Laboratory, April 1968.

3. Higgins, D. F., "The Diffraction of an Electromagnetic Plane Wave by Interior and Exterior Bends in a Perfectly Conducting Sheet," Sensor and Simulation Note 128, Air Force Weapons Laboratory, January 1971.

4. Cho, S. K., Chu, C. M., and Tai, C. T., "Prosimity Effect of Semi-infinite Parallel Plate Transmission Line in the Presence of a Perfectly Conducting Ground," Sensor and Simulation Note 137, Air Force Weapons Laboratory, August 1971.

5. Chu, C. M. and Cho, S. K., "Field Distribution for Parallel Plate Transmission Line of Finite Width in Proximity to a Conducting Plane," Sensor and Simulation Note 161, Air Force Weapons Laboratory, November 1972.

6. Merewether, D. E., "Transient Electromagnetic Fields Near a Cylindrical Antenna Multiply-Loaded with Lumped Resistors," Sensor and Simulation Note 71, Air Force Weapons Laboratory, August 1968.

7. Baum, C. E., "Resistively Loaded Radiating Dipole Based on a Transmission-Line Model for the Antenna, "Sensor and Simulation Note 81, April 1969.

8. Taylor, C. D. and Shumpert, T. H., "Electromagnetic Pulse Generation by an Impedance Loaded Dipole Antenna," Sensor and Simulation Note 104, November 1968.

9. Baum, C. E. and Chang, H., "Fields at the Center of a Full Circular TORUS and a Vertically Oriented TORUS on a perfectly Conducting Earth," Sensor and Simulation Note 160, Air Force Weapons Laboratory, December 1972.

10. Barnes, P. R., "Analytical Calculations of the Radiated Fields from the Vertical RES-I by the Application of Approximating Models," RES Memo Note 14, Air Force Weapons Laboratory, September 1969.

11. Wolff, E. A., Antenna Analysis, John Wiley and Sons, New York, 1966, p. 94.

12. Mei, K. K., "On the Integral Equations of Thin Wire Antennas," IEEE Trans. Ant. Prop., AP-13, pp. 374-378, May 1965.

13. Fyke, F. E., and C. M. Butler, "Characteristics of Loaded Rectangular Wire Loop Antennas," International USNC/URSI (VI), Boulder, Colorado; August, 1973.

14. Jones, D. S., The Theory of Electromagnetism, Pergamon Press, New York, 1964, p. 152.

15. Singaraju, B. K. and Baum, C. E., "Representative Measured Field Waveforms for ACHILLES II," ACHILLES Memos, Memo 8, Air Force Weapons Laboratory, May 1975.

16. Singaraju, B. K. and Baum, C. E., "Physical Description of ACHILLES II," ACHILLES Memos, Memo 7, Air Force Weapons Laboratory, April 1975.

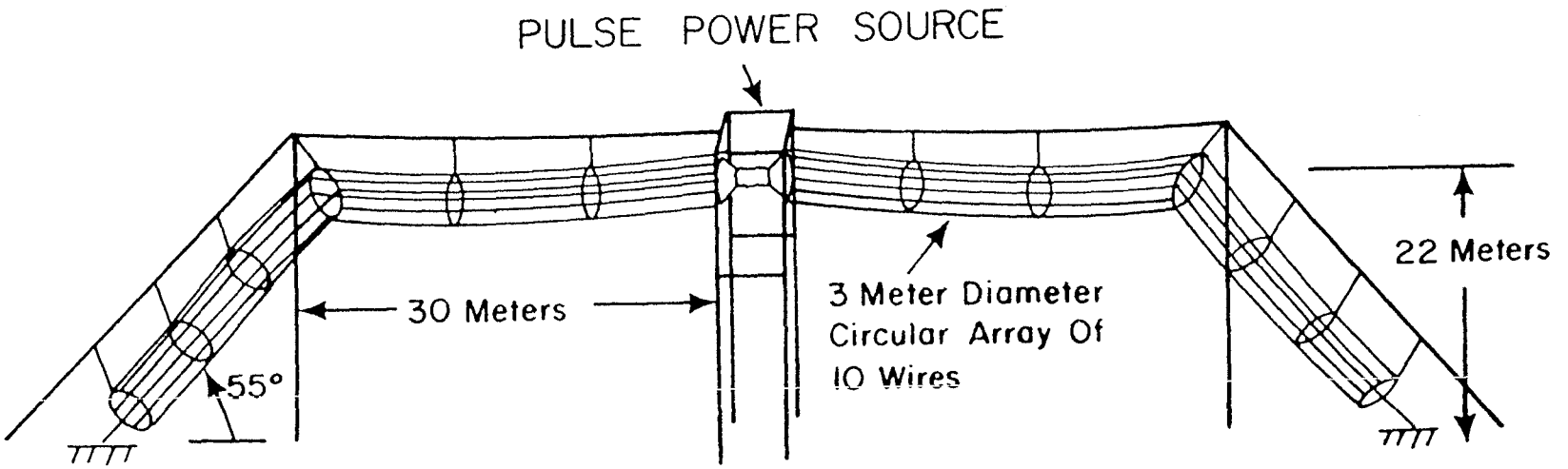

Figure 1: Illustration of the ACHILLES II EMP Simulator Facility, Kirtland AFB, New Mexico.

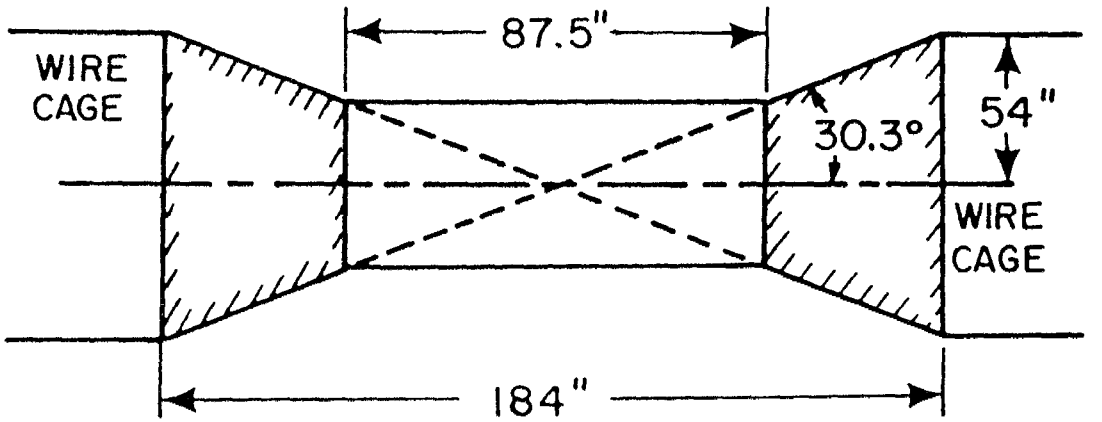

Figure 2: Conical Input Section for the ACHILLES II Simulator Facility.

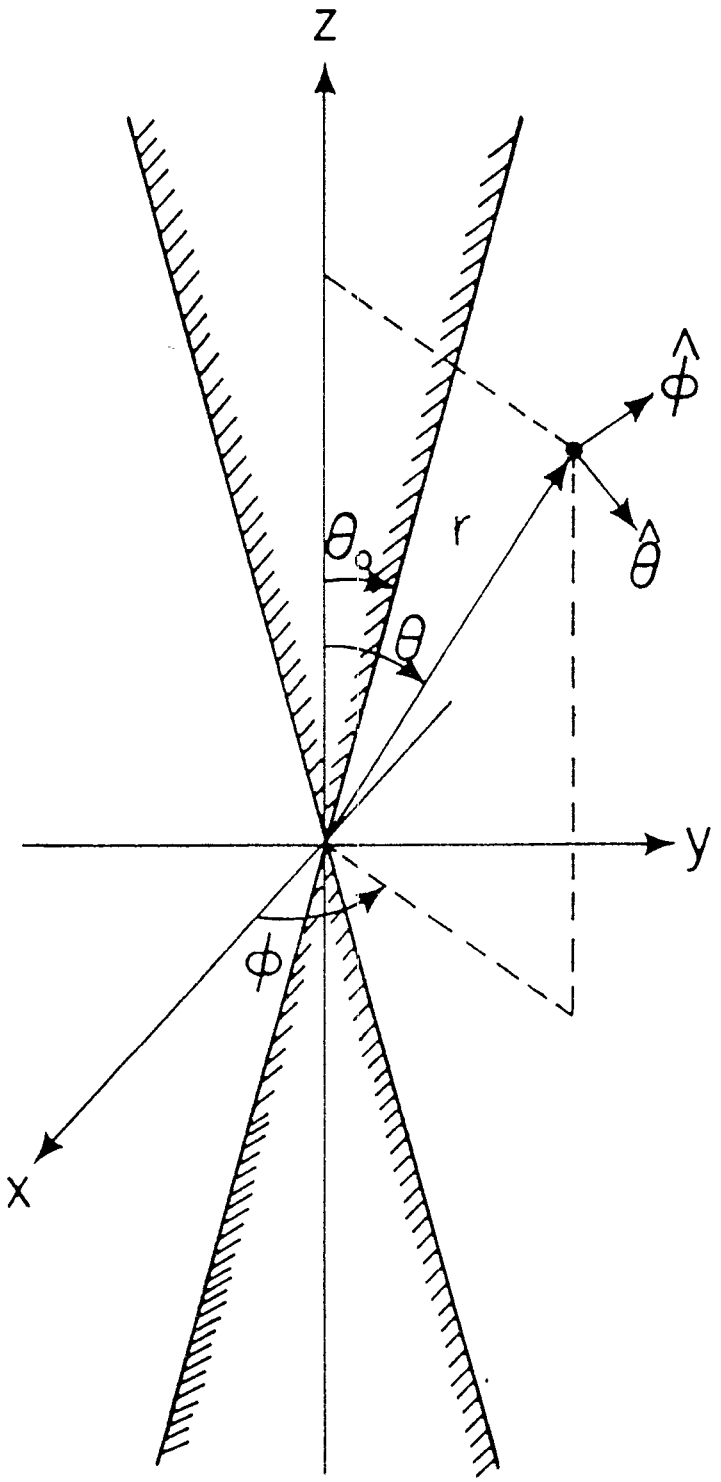

Figure 3: Biconical Antenna with a Spherical Cordinate System

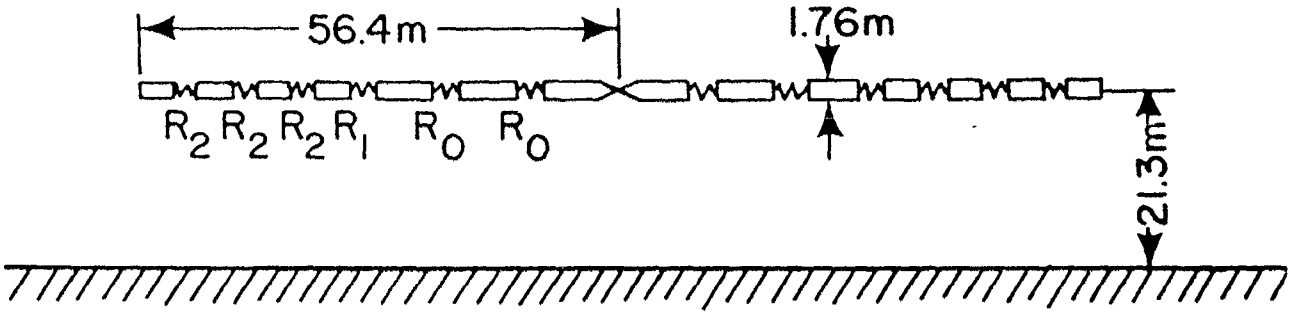

$R_0 = 45\Omega$

$R_1 = 46.2\Omega$

$R_2 = 47.8\Omega$

Figure 4: Resistively Loaded Cylinderical Antenna Oriented Horizontally Over a Ground Plane.

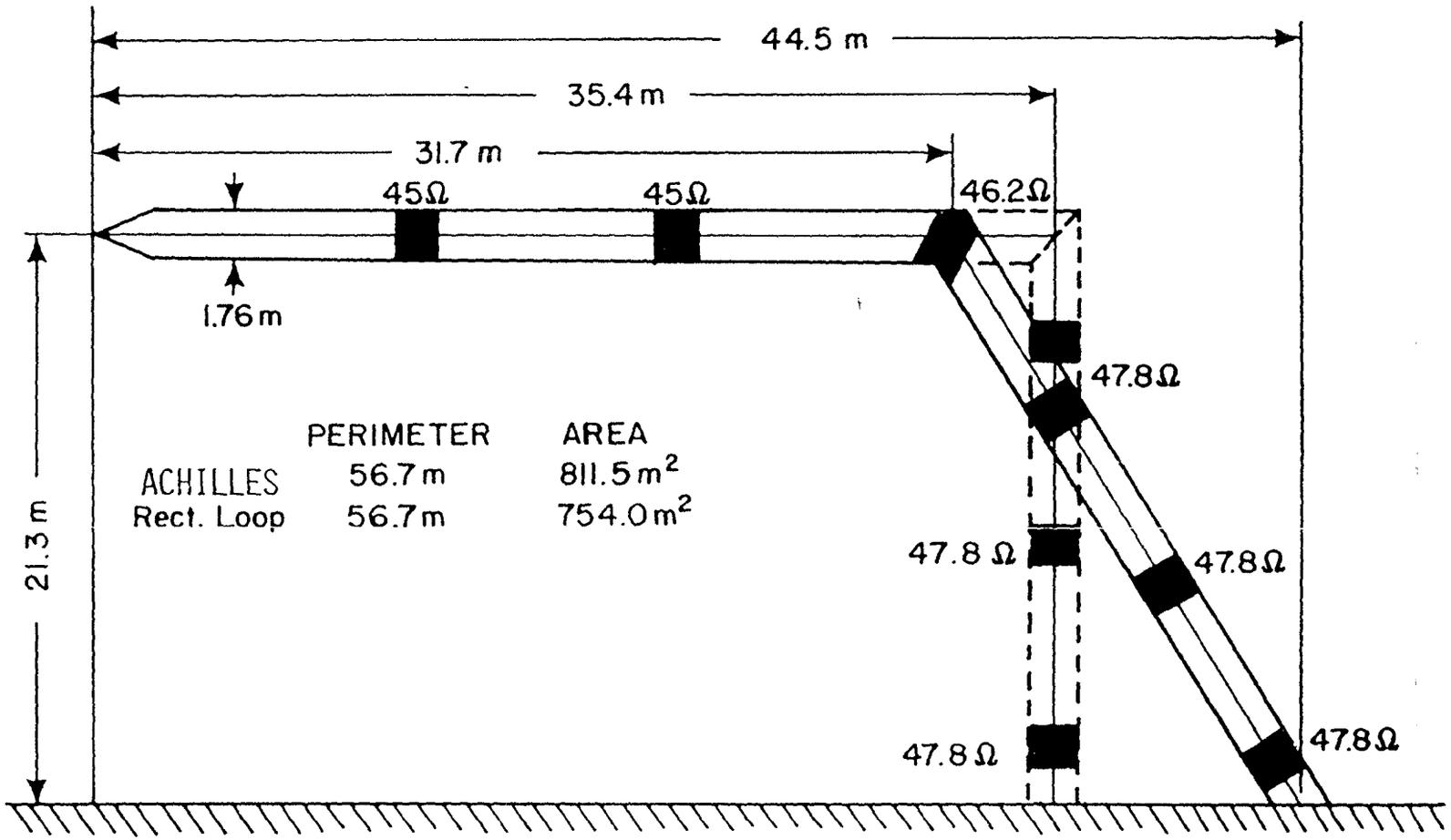

Figure 5: ACHILLES II Antenna with the Rectangular Loop Model Used in the Low Frequency Analysis.

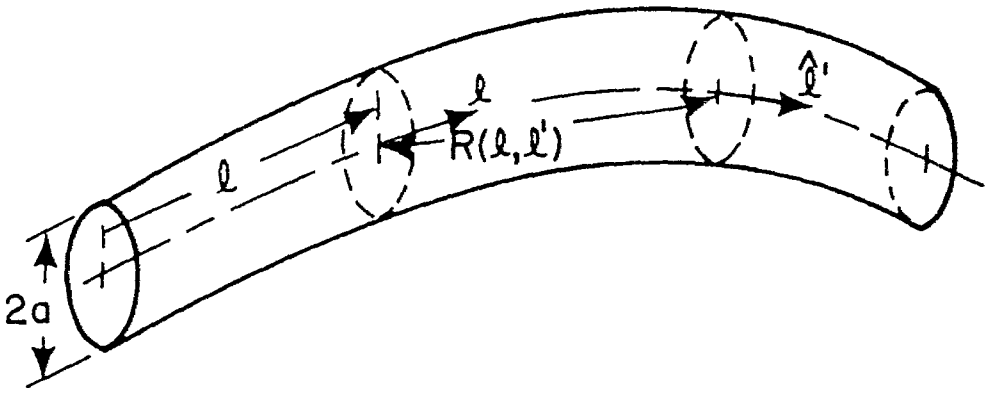

Figure 6: Arbitrarily Curved Wire

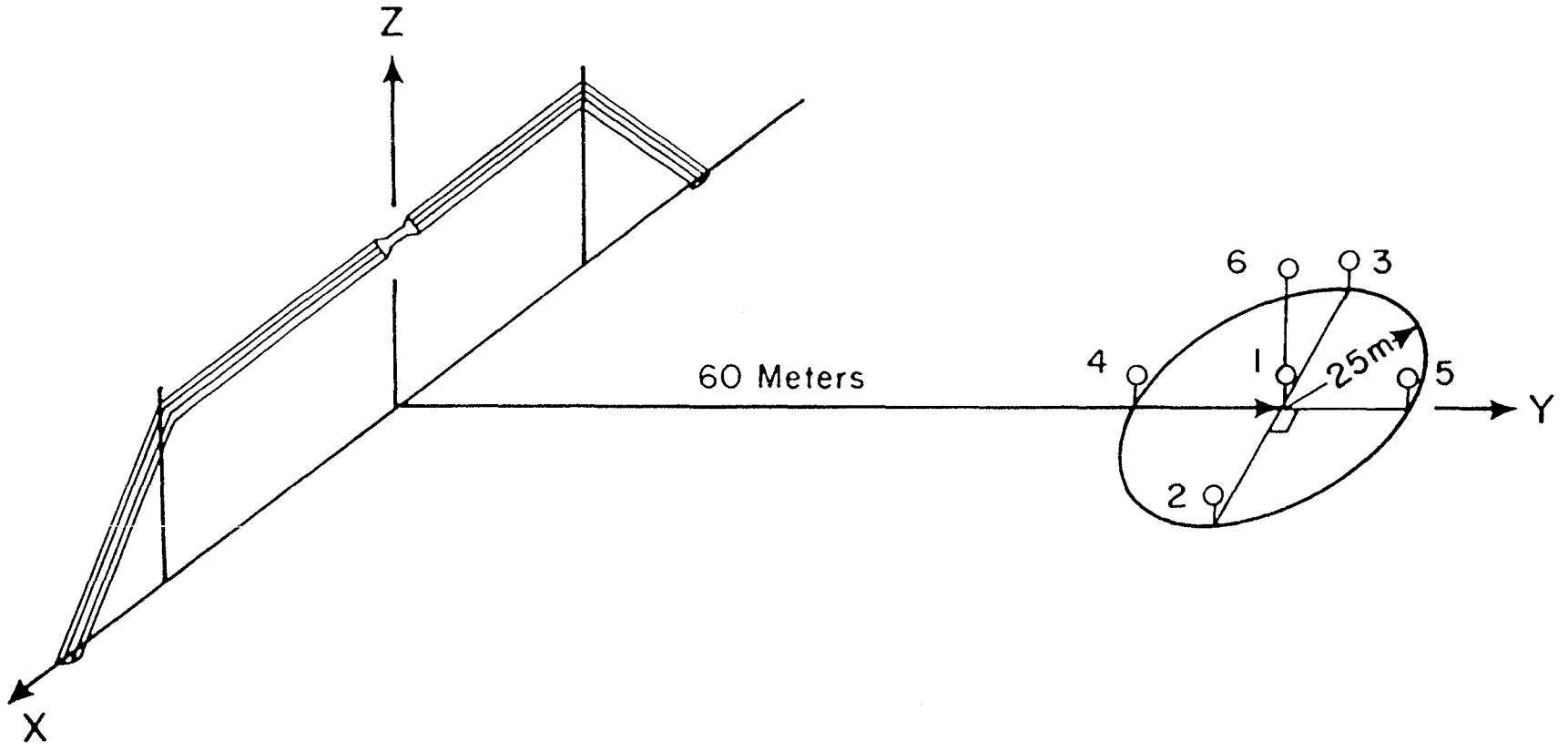

Figure 7: Location of the Field Points Used in Calculating the Electromagnetic Field Produced by the ACHILLES II Simulation, Pt1 = (0,60,2), Pt2 = (25,60,2), Pt3 = (-25,60,2), Pt4 = (0,35,2), Pt5 = (0,85,2), Pt6 = (0,60,12)

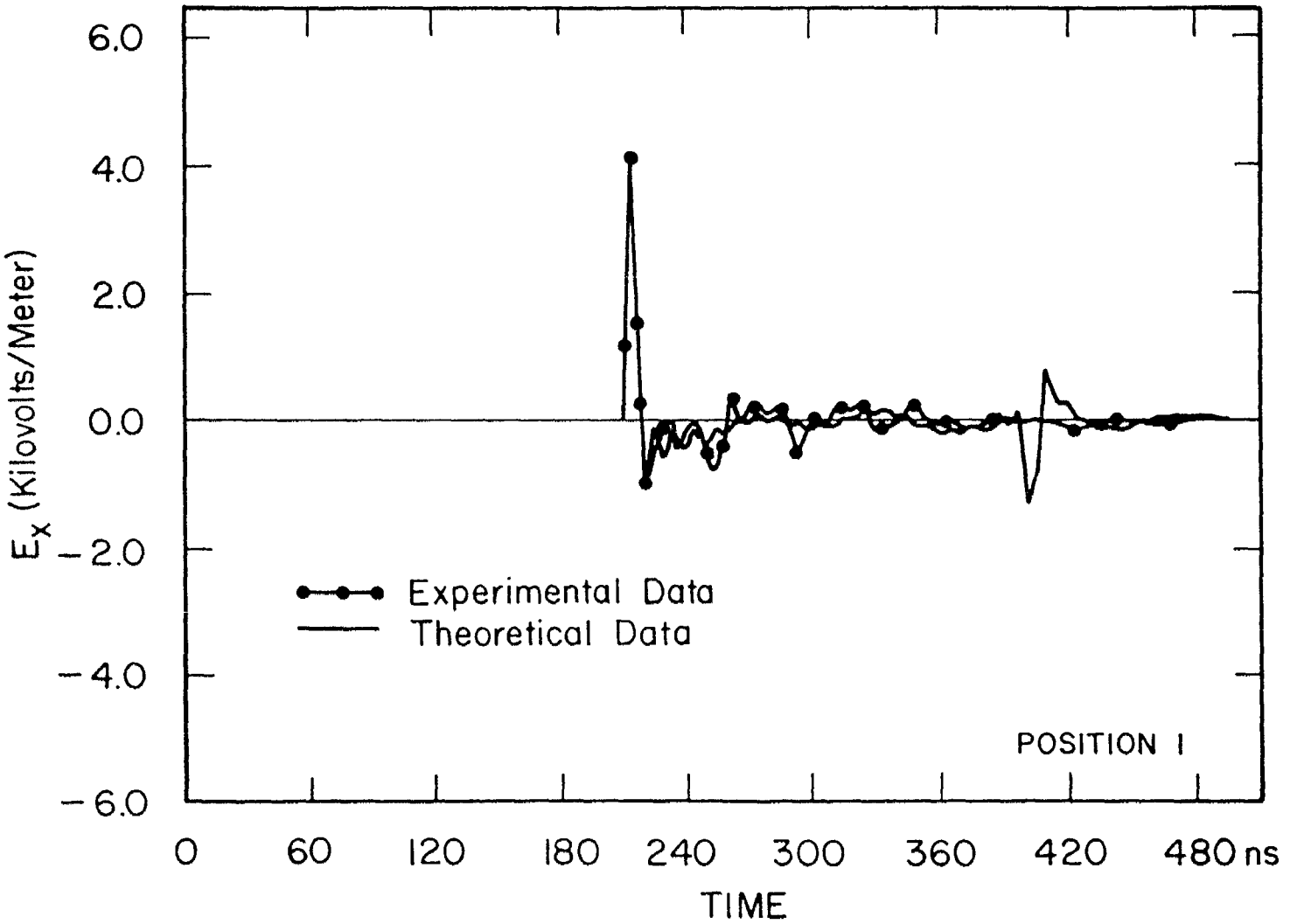

Figure 8: Measured versus Calculated Electric Field Pulse at Position 1

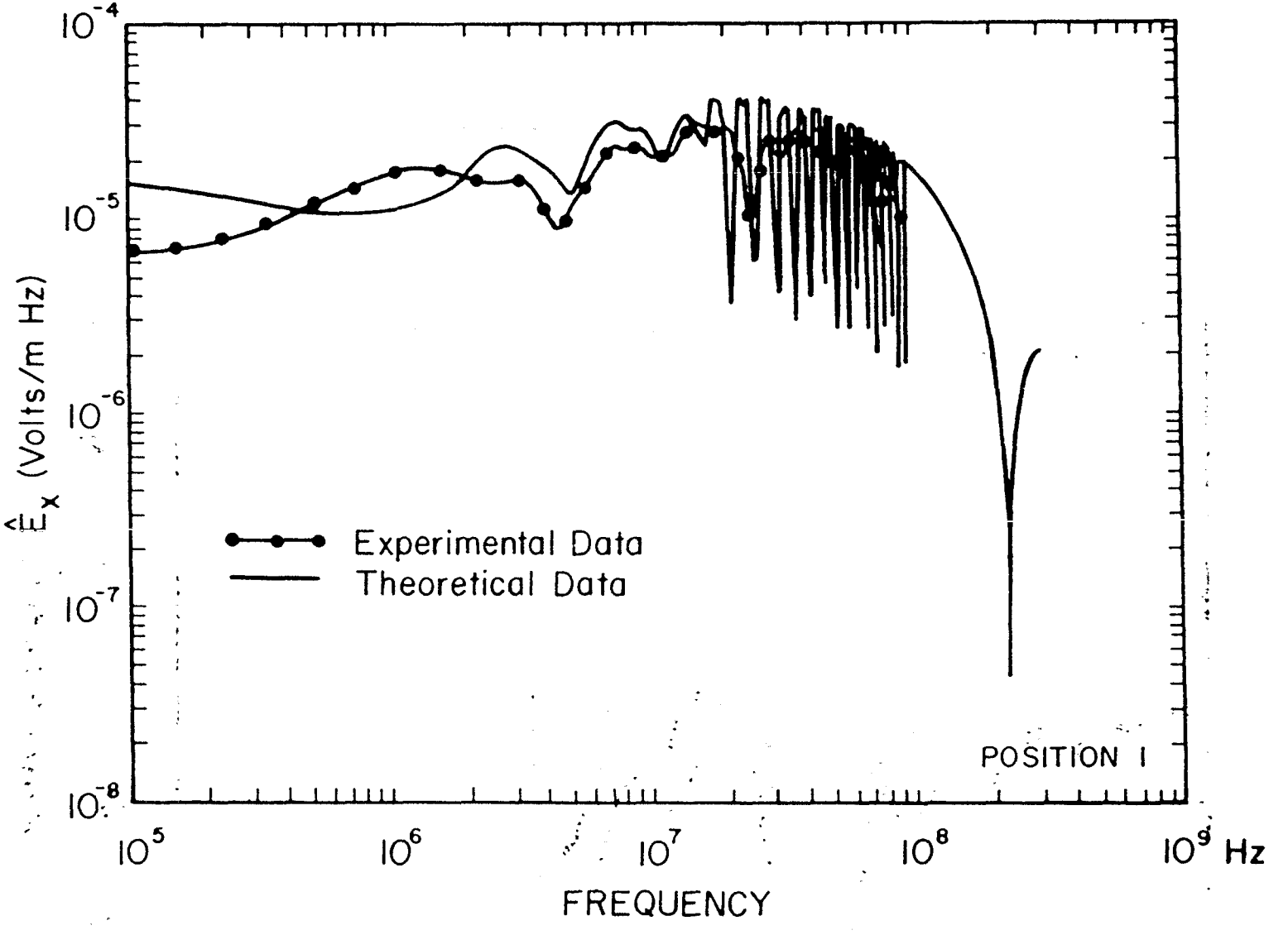

Figure 9: Fourier Transform of the Electric Field at Position 1

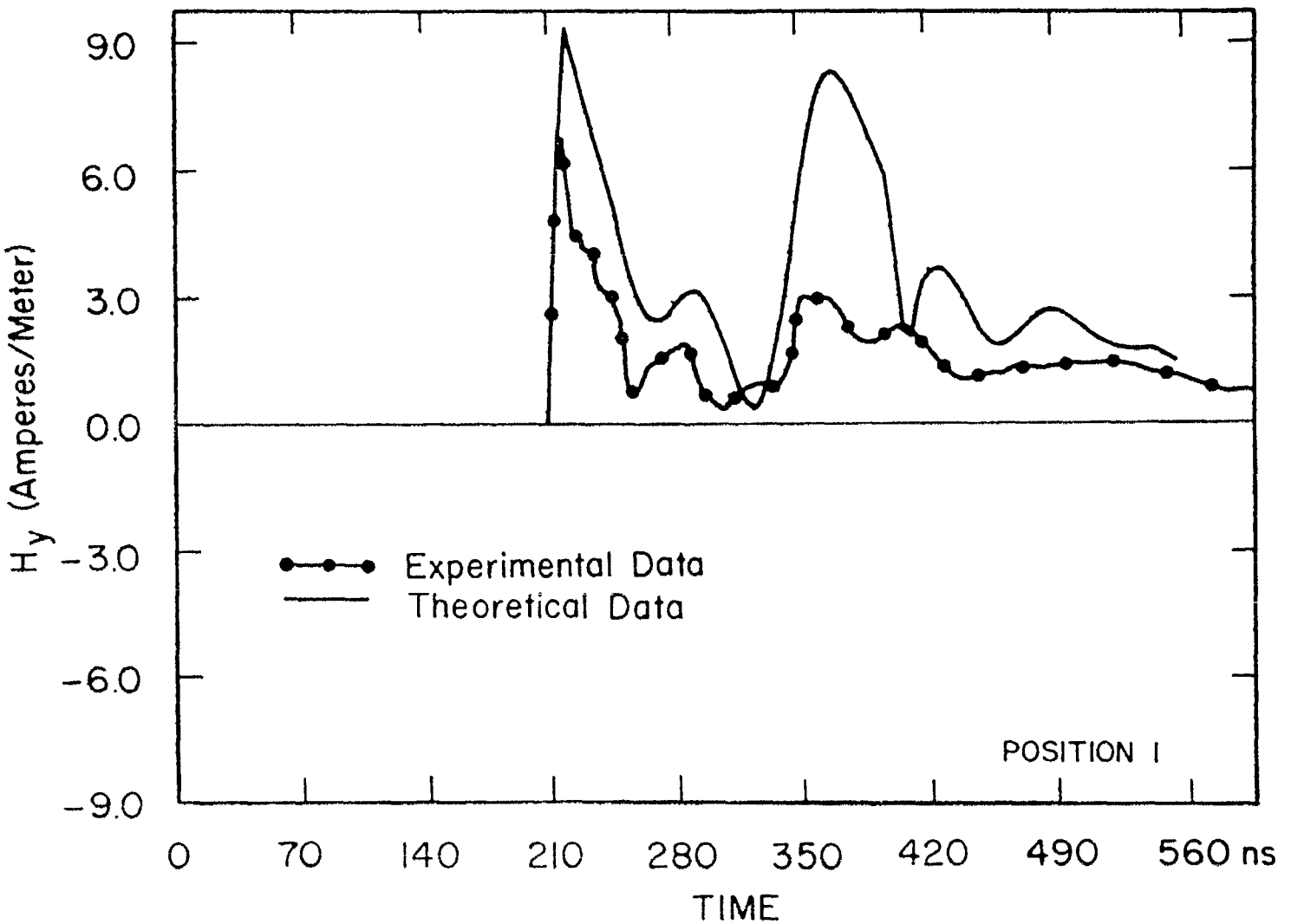

Figure 10: Measured versus Calculated Horizontal Magnetic Field Pulse at Position 1

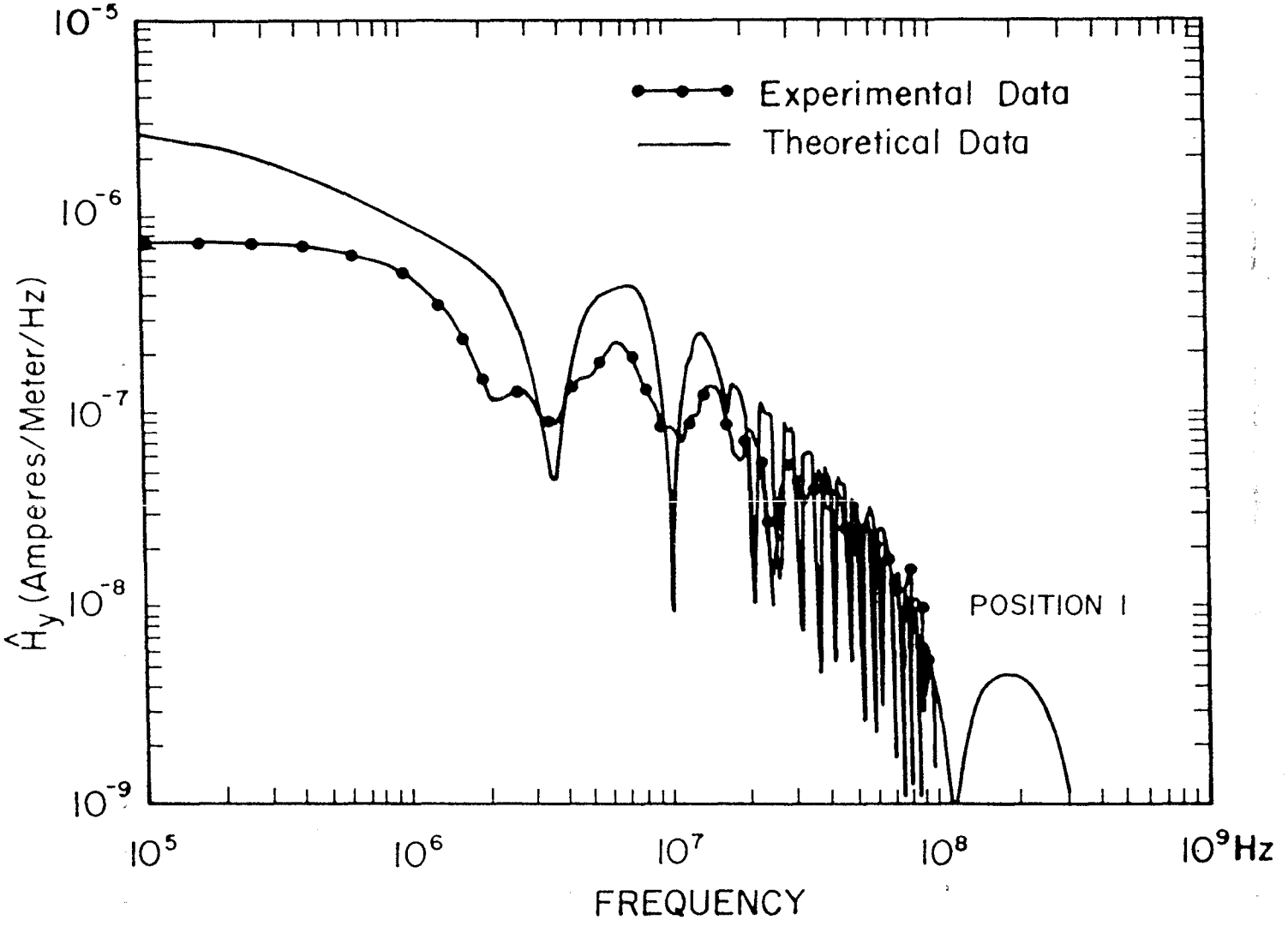

Figure 11: Fourier Transform of the Horizontal Magnetic Field at Position 1

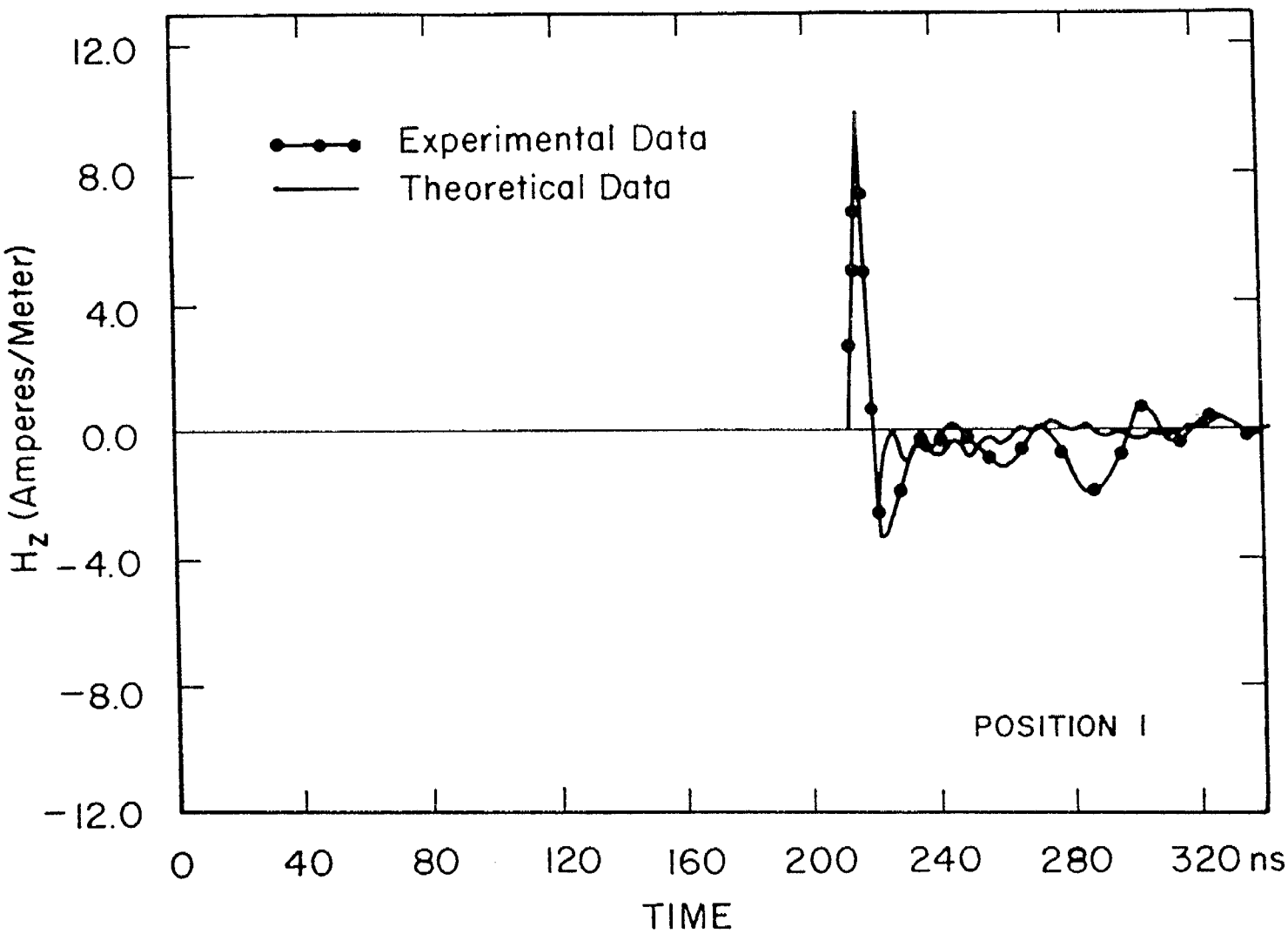

Figure 12: Measured versus Calculated Vertical Magnetic Field Pulse at Position 1

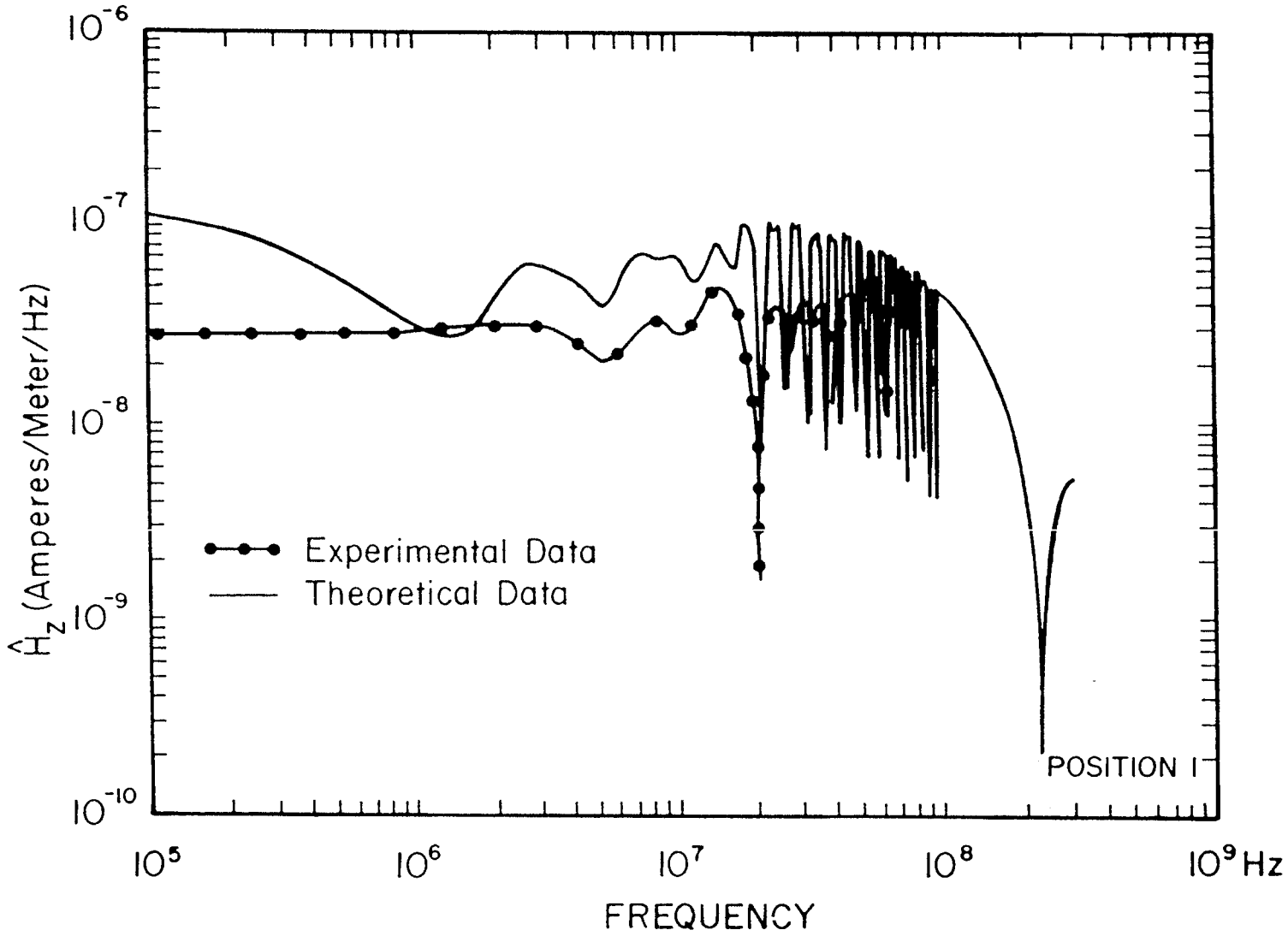

Figure 13: Fourier Transform of the Vertical Magnetic Field at Position 1

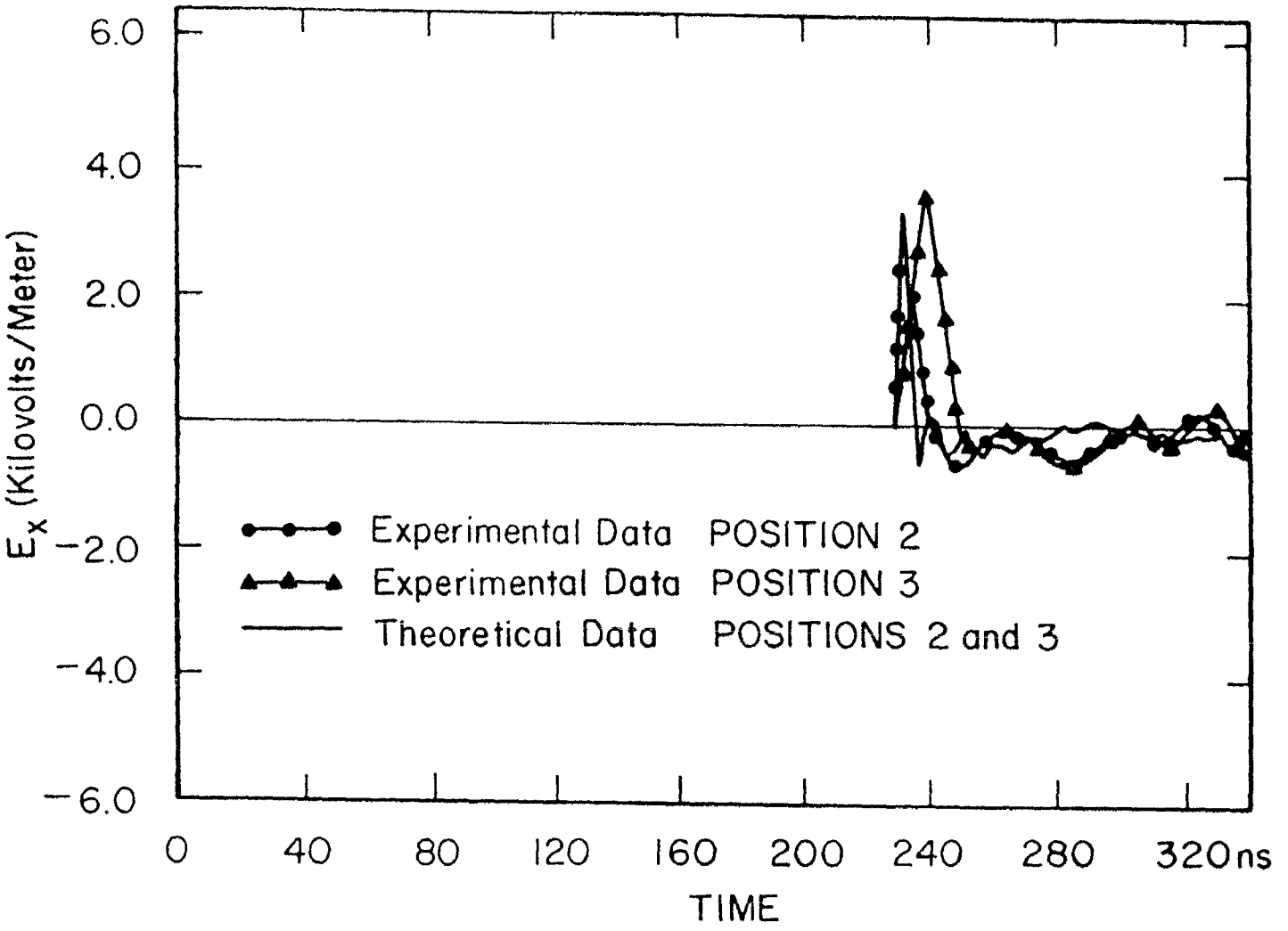

Figure 14: Measured versus Calculated Electric Field Pulse at Positions 2 and 3

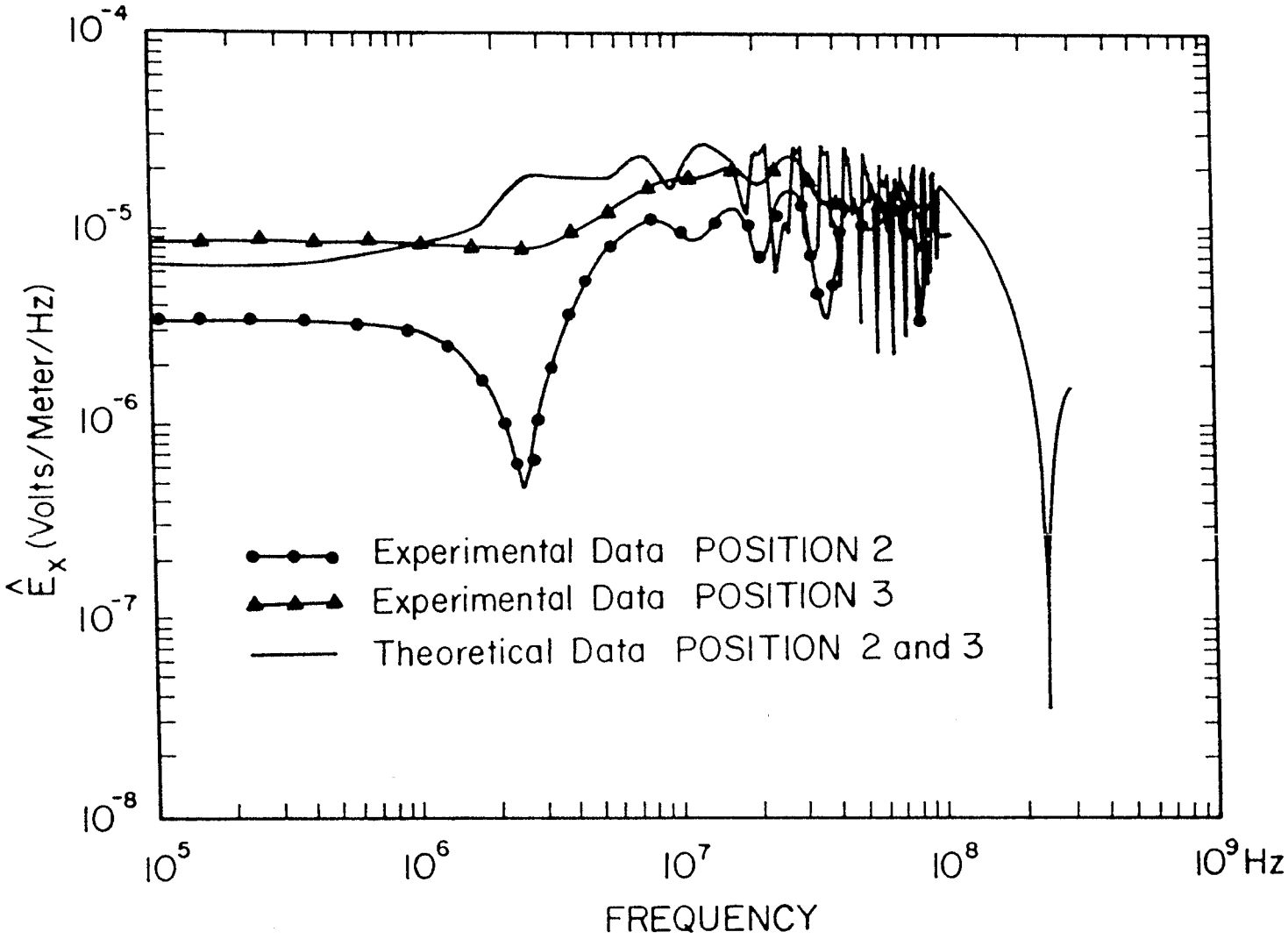

Figure 15: Fourier Transform of the Electric Field at Positions 2 and 3

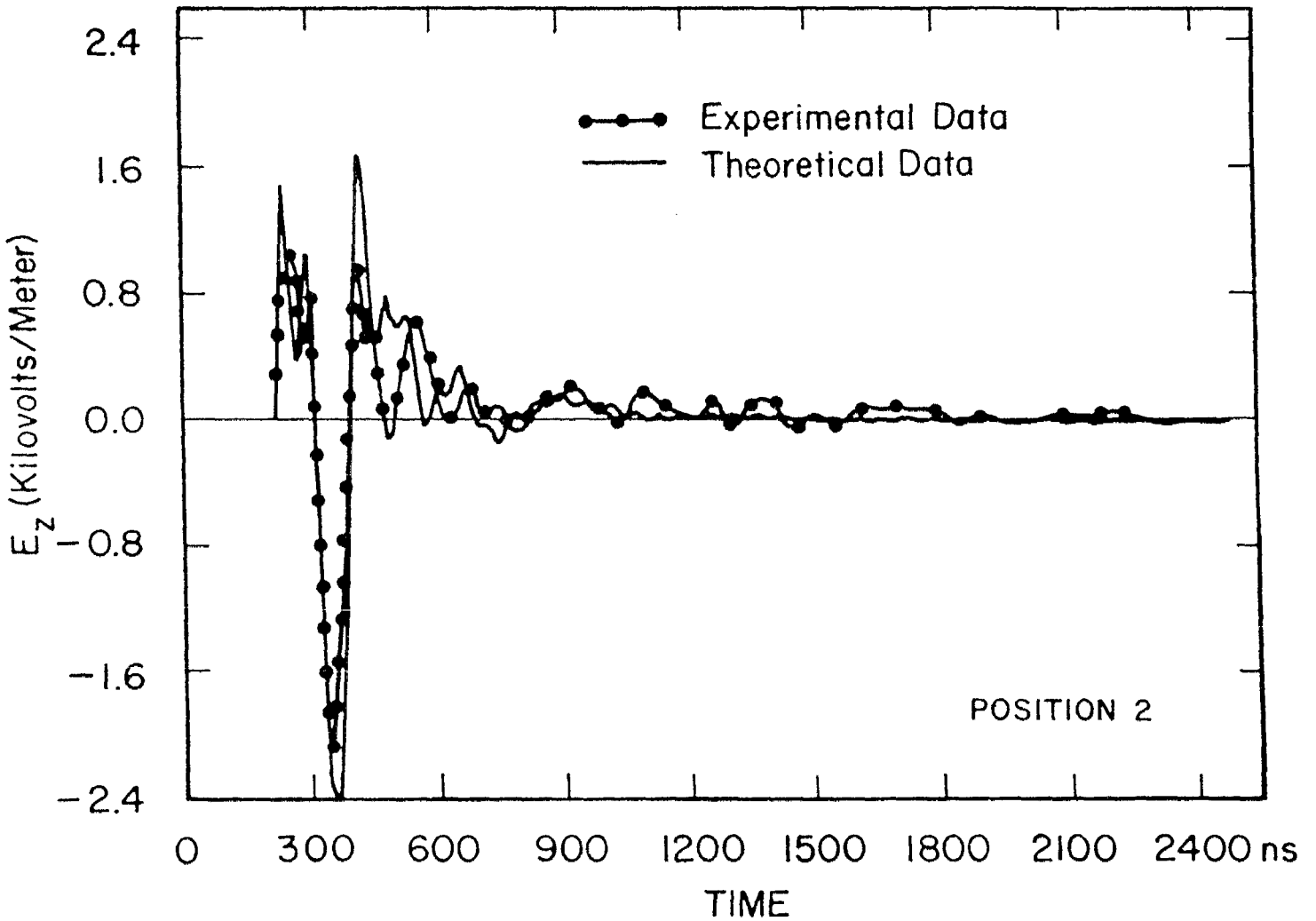

Figure 16: Measured versus Calculated Vertical Electric Field Pulse at Positions 2 and 3

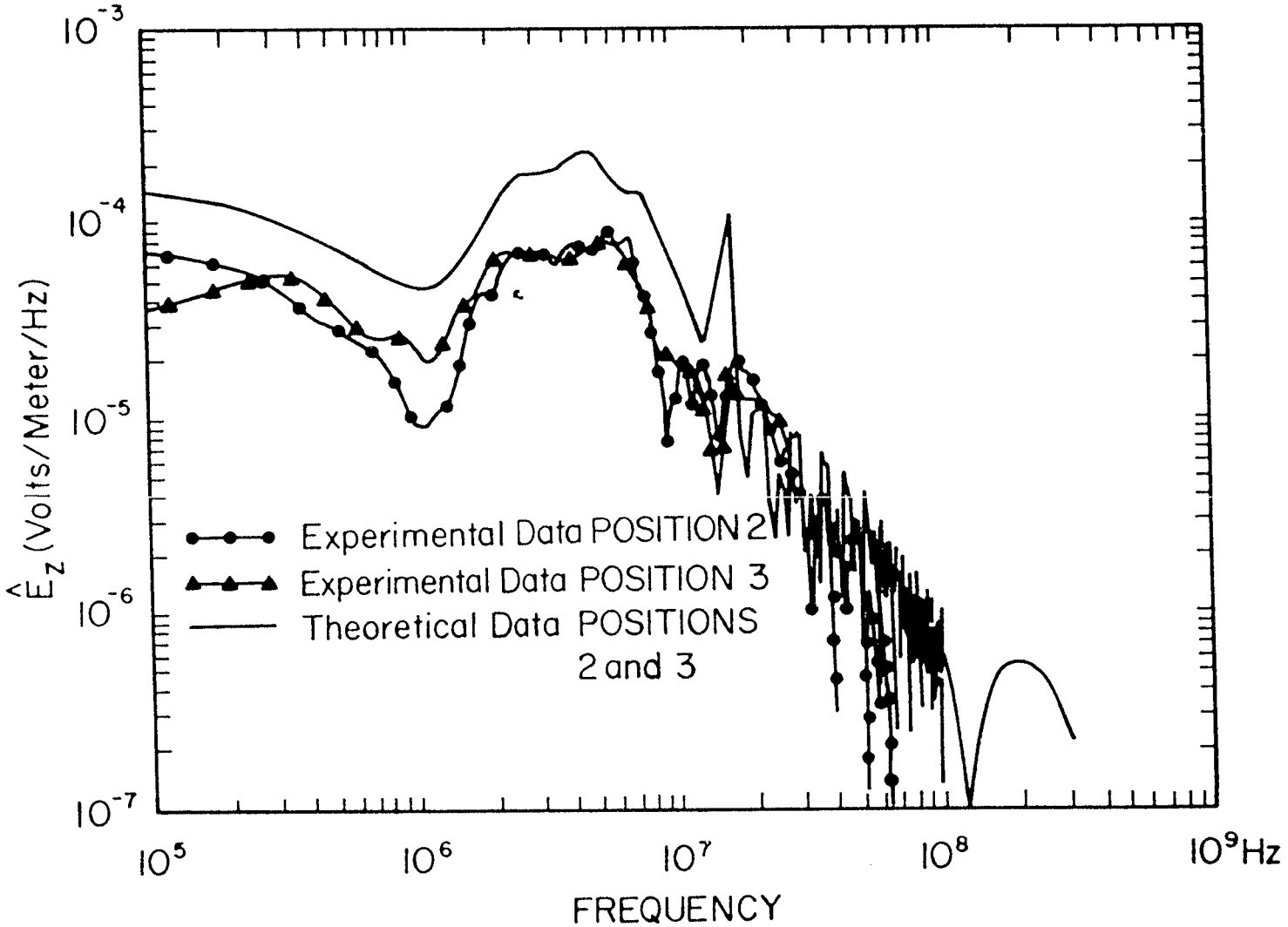

Figure 17: Fourier Transform of the Vertical Electric Field at Positions 2 and 3

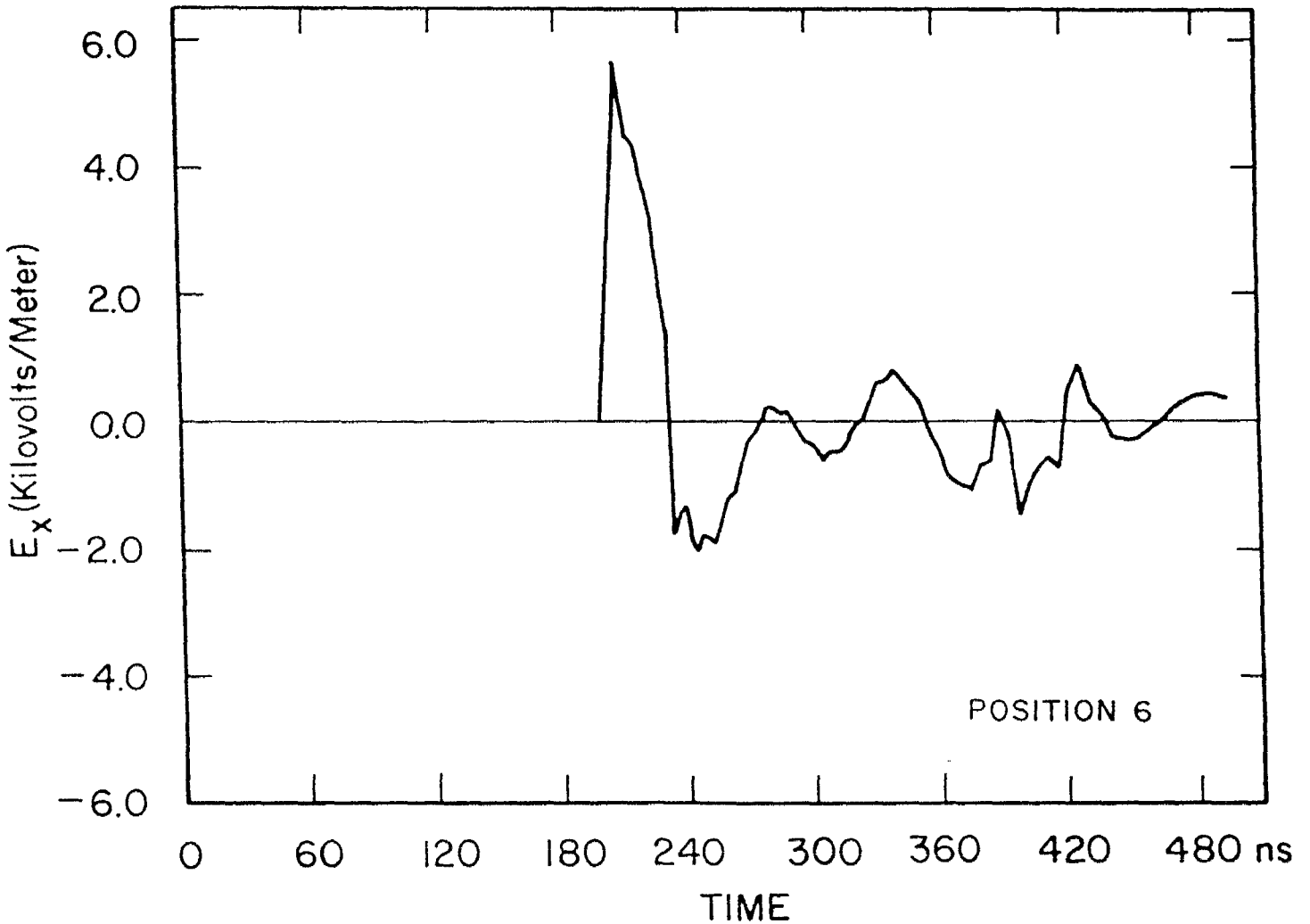

Figure 18: Calculated Electric Field Pulse at Position 6

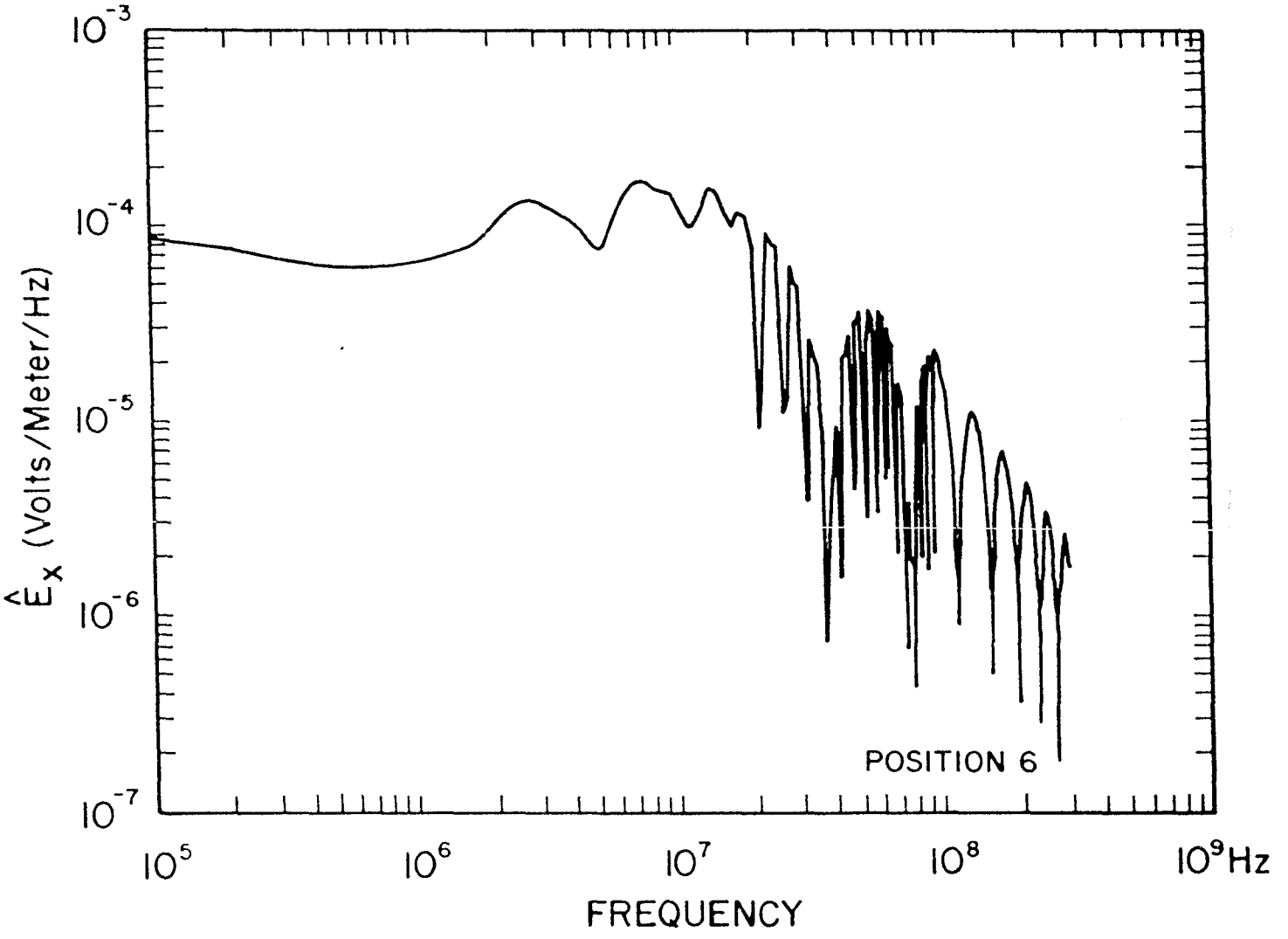

Figure 19: Fourier Transform of the Electric Field at Position 6

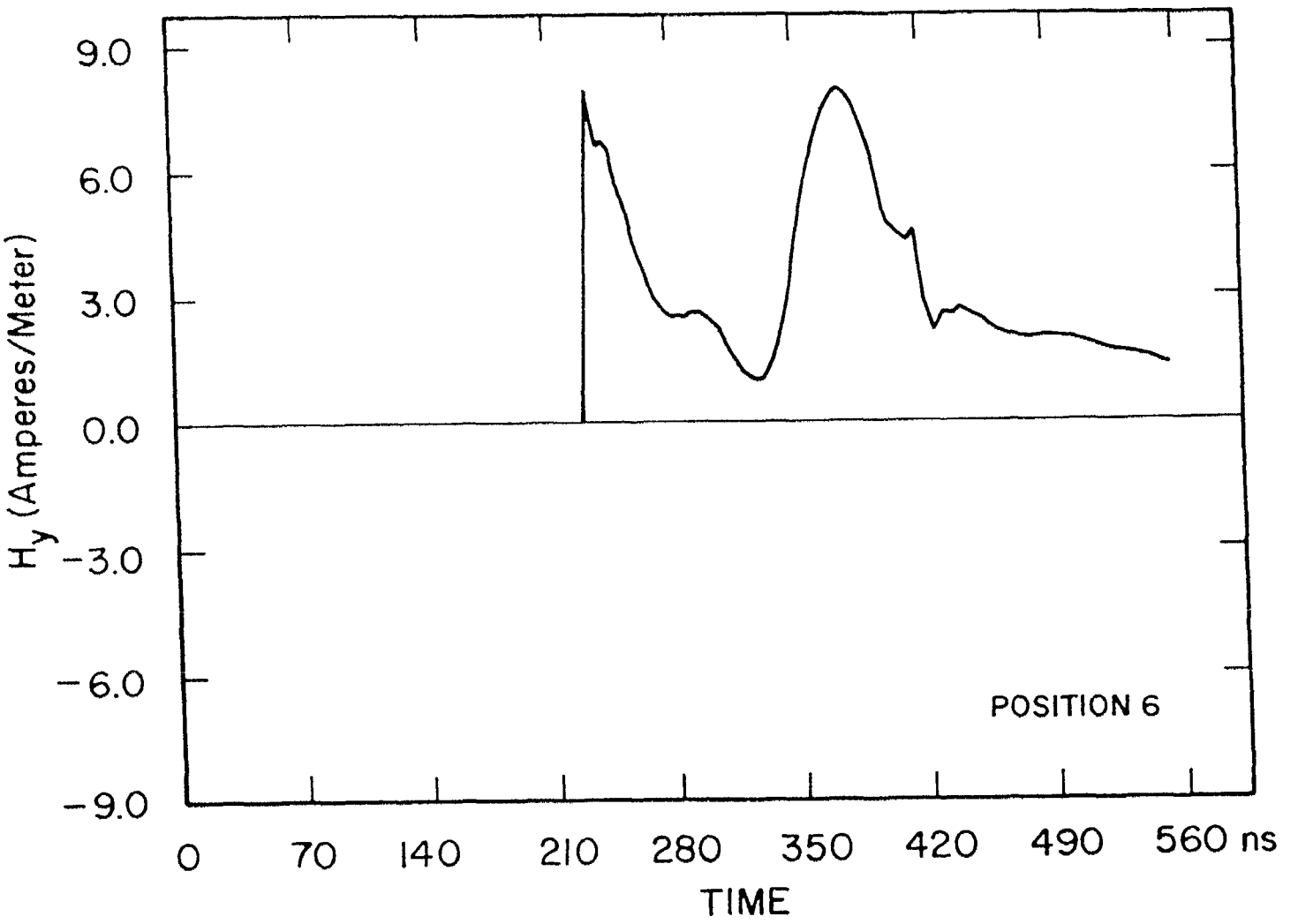

Figure 20: Calculated Horizontal Magnetic Field Pulse at Position 6

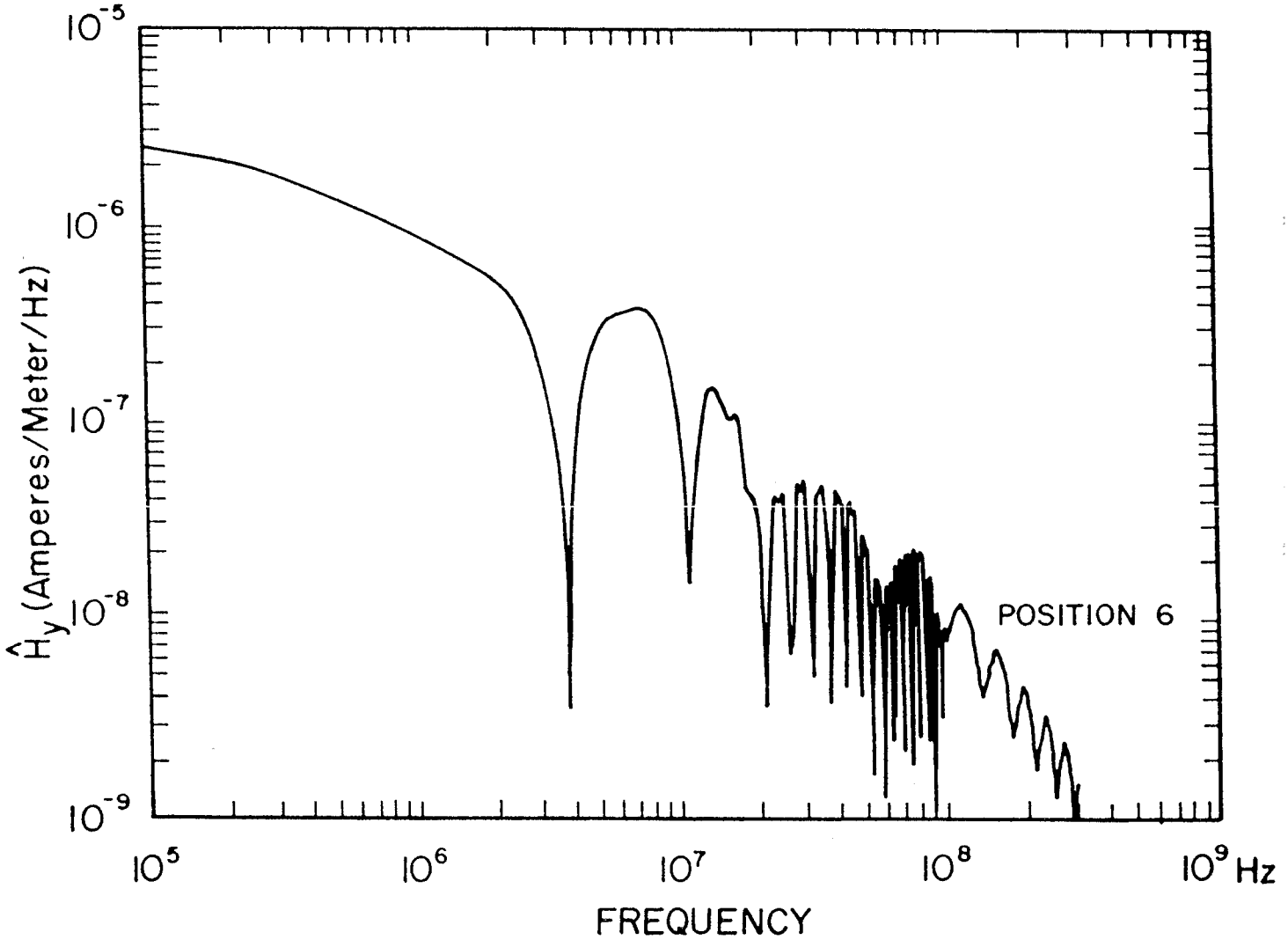

Figure 21: Fourier Transform of the Horizontal Magnetic Field at Position 6

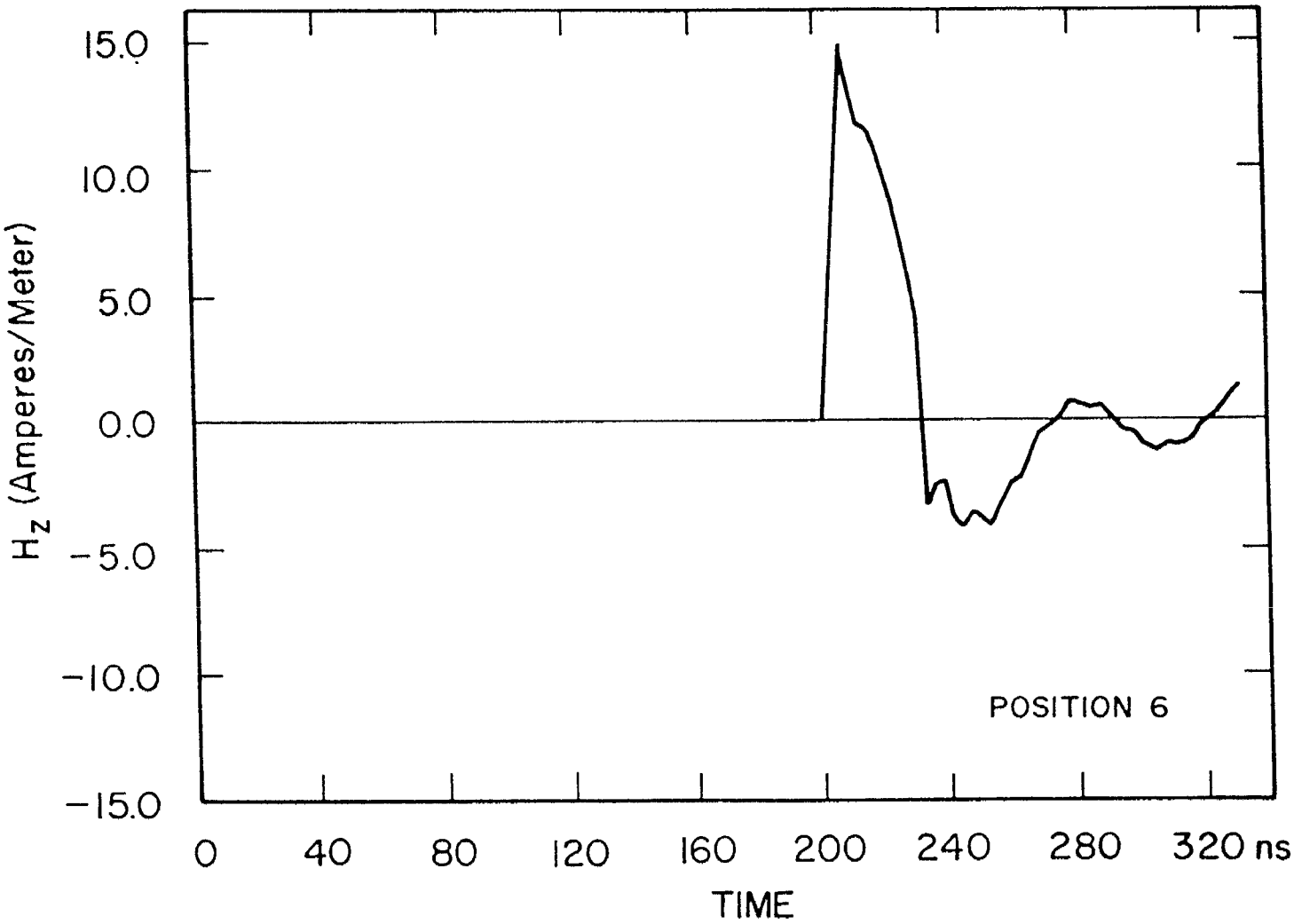

Figure 22: Calculated Vertical Magnetic Field Pulse at Position 6

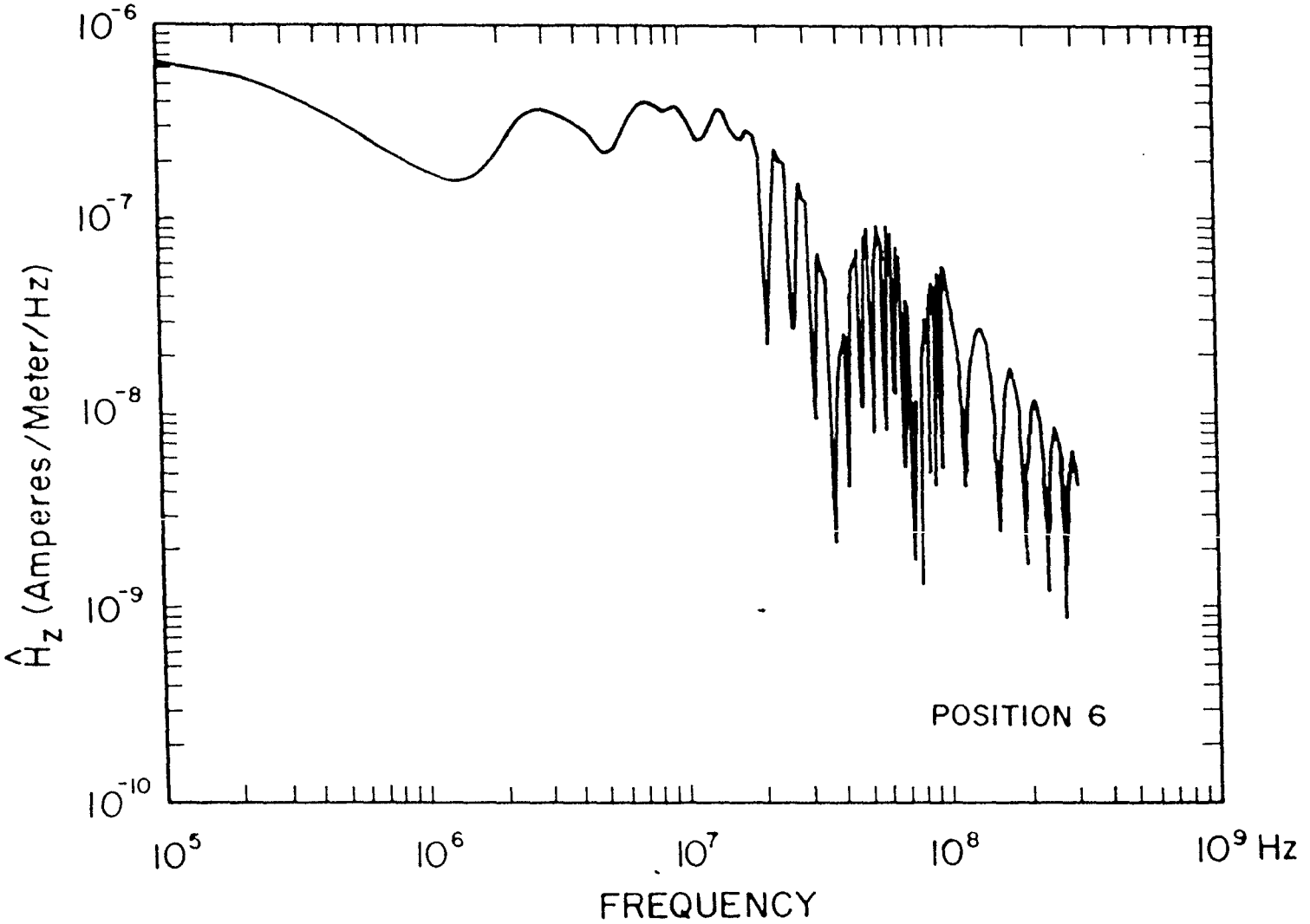

Figure 23: Fourier Transform of the Vertical Magnetic Field at Position 6